Received: 7 May 2021 | Revised: 24 June 2022 | Accepted: 17 October 2022

DOI: 10.1111/gbi.12534

ORIGINAL ARTICLE

gebiology WILEY

A re-examination of the mechanism of whiting events: A new role for diatoms in Fayetteville Green Lake (New York, USA)

Chloe Stanton[1] | Ben Davis Barnes[1] | Lee R. Kump[1,2] | Julie Cosmidis[1,2]

[1]Department of Geosciences, The Pennsylvania State University, University Park, Pennsylvania, USA

[2]Earth and Environmental Systems Institute, The Pennsylvania State University, University Park, Pennsylvania, USA

Correspondence
Julie Cosmidis, Department of Earth Sciences, University of Oxford, Oxford OX1 3AN, UK.
Email: julie.cosmidis@earth.ox.ac.uk

Present address
Julie Cosmidis, Department of Earth Sciences, University of Oxford, Oxford, UK

Funding information
Penn State Energy and Environmental Sustainability Laboratories; Pennsylvania Space Grant Consortium

Abstract

Whiting events—the episodic precipitation of fine-grained suspended calcium carbonates in the water column—have been documented across a variety of marine and lacustrine environments. Whitings likely are a major source of carbonate muds, a constituent of limestones, and important archives for geochemical proxies of Earth history. While several biological and physical mechanisms have been proposed to explain the onset of these precipitation events, no consensus has been reached thus far. Fayetteville Green Lake (New York, USA) is a meromictic lake that experiences annual whitings. Materials suspended in the water column collected through the whiting season were characterized using scanning electron microscopy and scanning transmission X-ray microscopy. Whitings in Fayetteville Green Lake are initiated in the spring within the top few meters of the water column, by precipitation of fine amorphous calcium carbonate (ACC) phases nucleating on microbial cells, as well as on abundant extracellular polymeric substances (EPS) frequently associated with centric diatoms. Whiting particles found in the summer consist of 5–7 μm calcite grains forming aggregates with diatoms and EPS. Simple calculations demonstrate that calcite particles continuously grow over several days, then sink quickly through the water column. In the late summer, partial calcium carbonate dissolution is observed deeper in the water column. Settling whiting particles, however, reach the bottom of the lake, where they form a major constituent of the sediment, along with diatom frustules. The role of diatoms and associated EPS acting as nucleation surfaces for calcium carbonates is described for the first time here as a potential mechanism participating in whitings at Fayetteville Green Lake. This mechanism may have been largely overlooked in other whiting events in modern and ancient environments.

KEYWORDS
biomineralization, calcite, calcium carbonates, diatoms, EPS, micrite, Whitings

1 | INTRODUCTION

Fine-grained (micritic) limestone is abundant in the sedimentary record and an important repository for geochemical and isotopic proxy records of Earth history. Despite its importance, the origin of marine mud has been a topic of considerable uncertainty and research for decades (Bathurst, 1966), with both inorganic and biogenic mechanisms being proposed. One source of mud, the apparently spontaneous precipitation of very fine suspended calcium carbonate ($CaCO_3$) particles, called whiting, has been observed to occur and persist for many days in marine environments, most notably in the Bahamas (Broecker & Takahashi, 1966; Larson & Mylroie, 2014; Purkis et al., 2017; Robbins et al., 1997; Shinn et al., 1989) and more recently in South West Florida (Long et al., 2014, 2017). Whiting events have also been described in different lacustrine environments (Dittrich & Obst, 2004; Hodell et al., 1998; Schultze-Lam et al., 1997). Physical disturbance and resuspension of bottom carbonate sediments by fish, sharks, tide, or wind (e.g., Boss & Neumann, 1993; Broecker, 2012; Broecker et al., 2000; Dierssen et al., 2009; Shanableh et al., 2021), chemical precipitation, possibly on resuspended sediment particles acting as seeds (Brunskill, 1969; Morse et al., 2003), and biological mediation (e.g., Long et al., 2017; Robbins & Blackwelder, 1992; Swart et al., 2014; Thompson, 2000) have been proposed to explain the whiting phenomenon.

1.1 | Biological hypotheses for the origin of whitings

Among biological mechanisms, the role of photosynthetic microorganisms (in particular, cyanobacteria) has often been invoked for whiting production, supported by the fact that whiting events often coincide spatially and temporally with high abundances of these organisms (Dittrich et al., 2004; Dittrich & Obst, 2004; Hodell et al., 1998; Schultze-Lam et al., 1997; Thompson, 2000). Biological models for the onset of whitings frequently involve the heterogeneous nucleation of $CaCO_3$ minerals on microbial surfaces in supersaturated waters (Robbins et al., 1996; Robbins & Blackwelder, 1992; Robbins & Yates, 1992; Schultze-Lam et al., 1992; Thompson, 2000). Picocyanobacteria in particular, because of their small sizes, offer a larger surface area for $CaCO_3$ nucleation (Dittrich et al., 2004; Dittrich & Obst, 2004; Hodell et al., 1998; Robbins & Blackwelder, 1992). Some studies have focused more specifically on the role of the S-layer of picocyanobacteria of the genus *Synechococcus*. Forming a hexagonally symmetric paracrystalline surface array, the S-layer may act as a template favoring calcite nucleation at the cell surface (Schultze-Lam et al., 1992, 1997; Thompson, 2000; Thompson & Ferris, 1990). Negatively charged organic functional groups such as carboxylates and phosphoryl groups, which are commonly present at the surface of the microbial cell wall or associated with extracellular polymeric substances (EPS), are also known to participate in $CaCO_3$ nucleation through the adsorption of Ca^{2+} cations (Dupraz & Visscher, 2005; Görgen et al., 2021), but the roles of such interactions have not been directly investigated in the context of whitings.

In addition to models based on $CaCO_3$ nucleation on microbial surfaces, cyanobacteria and other photosynthetic organisms might also provoke whiting events by locally increasing supersaturation with respect to calcium carbonates through CO_2 uptake (Dittrich & Obst, 2004; Schultze-Lam et al., 1997; Thompson, 2000). Recently, Lisle and Robbins (2016) hypothesized that viral lysis of cyanobacterial cells releases cytoplasmic bicarbonate—which is 23 times more concentrated in the cytoplasm than in seawater—leading to extreme mineral supersaturation in the immediate vicinity of the cells and enabling homogeneous nucleation of $CaCO_3$.

Other mechanisms for microbial precipitation of $CaCO_3$ minerals have been described in the literature dealing with calcifying microbial mats and microbialites (e.g., Dupraz et al., 2009; Dupraz & Visscher, 2005; Zhu & Dittrich, 2016). Some of these mechanisms, such as bacterial sulfate reduction or anoxygenic photosynthesis, are less likely to apply to whiting events, which occur in the oxygenated photic zone of the water column. Others, such as the degradation of microbial EPS locally releasing calcium and carbonate ions (e.g., Glunk et al., 2011), could be relevant to planktonic $CaCO_3$ formation, but it is not clear whether such mechanisms could be playing a role in the onset of whitings. Finally, some cyanobacteria (Benzerara et al., 2014) as well as other bacterial types (Benzerara et al., 2021; Monteil et al., 2021) and microalgae (Martignier et al., 2017) can form amorphous intracellular calcium carbonate biominerals, but their involvement in whiting events has never been documented.

1.2 | A role of diatoms in whitings?

Several studies have described an association of planktonic and benthic $CaCO_3$ precipitation with diatom species in different marine and lacustrine environments (Ehrlich et al., 2016; Fuchs et al., 2016; Gomez et al., 2018; Küchler-Krischun & Kleiner, 1990; Long et al., 2017; Winsborough, 2000; Winsborough & Golubić, 1987). Diatoms can produce large amounts of EPS, also called mucilage, playing different roles such as adhesion, motility, protection, and heavy metals detoxification (Shnyukova & Zolotareva, 2015; Urbani et al., 2012). In oligotrophic hard water lakes, diatoms have been observed in increasing numbers, causing ecological strain (Kirkwood et al., 2007; Novis et al., 2017), and their abundance sometimes coincides with increased sedimentation of $CaCO_3$ (Fuchs et al., 2016; Stabel, 1986). In at least one marine environment (South West Florida), $CaCO_3$ whiting particles were found associated with centric diatoms (Long et al., 2017), but it is unclear whether diatoms or their EPS could be a significant factor in calcium carbonate precipitation in other modern whiting events.

1.3 | Whiting events at Fayetteville Green Lake

Fayetteville Green Lake (FGL) (NY, United States) is a 53 m deep, permanently stratified lake where annual whitings have been

documented. The lake redoxcline at ~20 m water depth separates an upper, wind-mixed, oxygenated mixolimnion from a lower, slightly denser, euxinic monimolimnion (Takahashi et al., 1968). The upper mixolimnion of FGL is supersaturated with respect to calcite ($\Omega \approx 10$) (Takahashi et al., 1968), and experiences a whiting every spring and summer (May–August), when precipitation of fine-grained suspended calcite transforms the lake color from deep blue to turquoise (Schultze-Lam et al., 1997; Thompson et al., 1990). Sediment resuspension can be ruled out as a cause of whiting at FGL due to the significant depth and meromictic nature of the lake, so previous studies of the FGL whitings have focused on possible biological mechanisms.

Carbon stable isotope measurements suggest an important contribution of photosynthesis to the isotopic composition of carbonate minerals present in the lake sediments (Havig et al., 2017; Schultze-Lam et al., 1997). Primary production in FGL mixolimnion is dominated by coccoid picocyanobacteria of the genus *Synechococcus* (Kamennaya et al., 2020; Thompson et al., 1990) as well as centric and pennate diatoms (Schultze-Lam et al., 1997). A model for the onset of the whiting has been proposed in the 1990s, in which *Synechococcus*, which outnumber diatoms by five orders of magnitude in the surface waters of FGL (Schultze-Lam et al., 1997), were the main biological agents driving $CaCO_3$ precipitation. The cyanobacteria are thought to be driving local increases in calcium carbonate saturation state from their photosynthetic activity and acting as sites for mineral nucleation (Schultze-Lam et al., 1997; Thompson et al., 1990).

Schultze-Lam et al. (1997) documented the seasonal evolution of the whiting and showed that the initiation of the whiting in the spring (May) roughly coincides with an annual cyanobacterial bloom. Although these authors also recorded a summer diatom bloom coinciding with the whiting at FGL, they discarded a possible involvement of diatoms in $CaCO_3$ formation due to the absence of calcite association with diatoms on electron microscopy images (Schultze-Lam et al., 1997). A *Synechococcus* strain isolated from FGL was furthermore shown in the laboratory to nucleate calcite crystals at the cell surface, possibly templated on the S-layer (Schultze-Lam et al., 1992; Thompson & Ferris, 1990). Recently, Kamennaya et al. (2020) have shown that *Synechococcus* thriving in the surface waters of FGL produce abundant EPS that can adsorb diverse cations (including calcium) and detach from the cells. However, it is not clear whether or not these cell-free calcium-loaded EPS envelopes play a role in $CaCO_3$ precipitation.

Other recent studies of FGL have focused on thrombolitic microbialites growing on the lake shore (DeMott et al., 2020; Uveges et al., 2018), isotopic fractionation effects associated with microbial calcite precipitation (Chen et al., 2021), as well as carbon and nitrogen biogeochemical cycling (Fulton et al., 2018; Havig et al., 2017), sulfur biogeochemistry (Oduro et al., 2013; Zerkle et al., 2010), and microbial and geochemical processes at the chemocline and in the monimolimnion (Block et al., 2021; Havig et al., 2015; Hunter, 2012; Meyer et al., 2011; Rojas et al., 2021).

In the present study, we performed a high-resolution microscopy and spectroscopy characterization of $CaCO_3$ particles suspended in the water column of FGL and collected through the whiting season, as well as of particles from the lake bottom sediments. Combined with geochemical profiles in the upper part of the mixolimnion, these analyses enable us to propose new hypotheses for the biological mechanisms involved in whiting events and carbonate sedimentation at FGL.

2 | METHODS

2.1 | Field sampling

Fieldwork was conducted during the spring, summer, and fall of 2018 at Green Lakes State Park, in Fayetteville, NY (United States). Five field trips were executed on April 16, May 31, June 30, August 1, and September 8, 2018. Samples were collected from a boat stationed near the lake center. Water samples were collected using a peristaltic pump at every 1 m interval for the top ~10 m of the water column. Both filtered (0.2 μm polycarbonate filters) and unfiltered water samples were collected and stored at 4°C. Water samples were analyzed within a few days for alkalinity determination, or within a maximum of 3 months for cation and anion measurements (see Section 2.2). Polycarbonate filters were immediately rinsed with deionized (DI) water, air-dried, and stored at 4°C for later microscopy analyses (see Section 2.3). Rinsing is not expected to have caused any substantial mineral dissolution, as evidenced by the absence of mineral pitting in samples collected in the spring. Sediment trap samples analyzed in this study were collected by S. Romaniello (University of Tennessee, Knoxville) between July 12 and July 21, 2017, from 13.5 depth, and stored at −20°C prior to analyses. Samples from the top 4 inches of an FGL bottom sediment core were also analyzed. These sediment core samples were freeze-dried for preservation. They have been further described elsewhere (Havig et al., 2015, 2017).

2.2 | Geochemical profiling

Vertical profiles of relevant physical and geochemical parameters were measured in each field trip through the top 25 m of the water column (total depth 53 m) using a YSI sonde (model 6600v2). Depth profiles were generated for temperature, conductivity, pH, and optical dissolved oxygen. Upon return to the laboratory, additional geochemical analyses were conducted for filtered water samples drawn from the upper ~10 m of the water column. Alkalinity was determined for each field trip using sulfuric acid autotitrations (Orion Star T910 pH Titrator), whereas major cation and anion concentrations were analyzed for June and September samples using inductively coupled plasma atomic emission spectroscopy (ICP-AES, Thermo Fisher ICAP 7400) and ion chromatography (IC, Dionex ICS-3000), respectively. PHREEQC (Parkhurst & Appelo, 2013) was used to estimate the calcite saturation index and dissolved carbonate chemistry of each water sample constrained by the alkalinity and pH field data. These simulations were supplemented with the cation and anion concentrations from both

June and September samples to test the sensitivity of FGL carbonate chemistry to minor seasonal changes in major-element chemistry. The PHREEQC code used for these calculations is available in Supplementary Information.

2.3 | Scanning electron microscopy (SEM)

Suspended particles from the water column and collected on polycarbonate filters, as well as sediment trap samples rinsed with DI water, were characterized using scanning electron microscopy (SEM) on an FEI Nova NanoSEM 630 field emission gun SEM. Elemental information was derived from Energy-dispersive X-ray Spectroscopy (EDS) (Oxford Instruments UltimMax detector) to confirm the mineralogy of observed particles. Images were collected at accelerating voltages ranging from 5 to 15 keV and at working distances down to 3 mm, while EDS analyses were conducted at 15 keV at working distances down to 7 mm. EDS data were processed using the program Oxford Aztec.

Mineral morphology and texture, size, and abundances, as well as diatom abundances, were assessed using SEM images generated throughout the whiting season by manual counting on ~700 µm x 700 µm SEM images of the filters. Three types of particles were counted and measured on these large-scale overview images: pennate diatoms, centric diatoms, and carbonate grains. The visual aspect of the carbonate particles was furthermore characterized as either intact or pitted (as indicative of dissolution). Once all particles on these larger images had been counted, the volumetric concentrations of each type of particle were calculated, using the volume of filtered water for each filter and filter area. The areas counted (~0.49 mm^2) were assumed to be representative of the entire filters (~490 mm^2), which contained all particles from the originally filtered 60 ml samples. Using these values, particle counts from the SEM images were converted into concentrations of particles per milliliter. This counting method relies on the assumption that particles are homogeneously distributed on each filter, which may be a source of error.

2.4 | Scanning transmission X-ray microscopy (STXM)

2.4.1 | STXM data acquisition and processing

Scanning Transmission X-ray Microscopy (STXM) was used to collect spectroscopic data on the sub-micrometer scale distribution and speciation of carbon and calcium in minerals and associated organics. STXM analyses were performed on beamline SM at the Canadian Light Source, Saskatoon, SK, operating with a 35 nm zone plate (ZP) on samples collected from the water column in April 2018. The STXM beamline 5.3.2.2 (operating with a 25 nm ZP) of the Advance Light Source, Berkeley National Lab, CA, was used to analyze sediment trap and sediment core samples. For STXM, particulate materials were centrifuged, rinsed with deionized water, and deposited onto silicon nitride windows (Norcada Inc.).

STXM data acquired at the C K-edge and Ca $L_{2,3}$-edge were processed in aXis2000 (Hitchcock, 2012). Transmission images were first converted to optical density (OD). At the C K-edge, organic carbon maps were generated by subtracting an OD image at 280 eV (below the C K-edge) from another at 288.2 eV (absorption energy of 1 s → $\pi^*_{C=O}$ electronic transitions in amide groups). Calcium maps were obtained at the Ca $L_{2,3}$-edge by subtracting an OD image at 343 eV (below the Ca L_3-edge) from another at 349.3 eV (energy of the Ca L_3-edge).

X-ray absorption near edge structure (XANES) spectra were extracted from image stacks according to the procedure described by Cosmidis and Benzerara (2014). The Stack Fit tool of aXis2000 was used to extract and map the distribution of representative components in image stacks. Linear background removal was performed on XANES spectra in the 270–283 eV energy range below the C K-edge and the 340–346 eV energy range below the Ca $L_{2,3}$-edge.

2.4.2 | Determination of I_C/I_{Ca} ratios

XANES spectra at the C K-edge and Ca $L_{2,3}$-edge were used to obtain a semi-quantitative measure of elemental ratios of carbon versus calcium in the samples. The I_C/Ic_a ratio is defined as the ratio of the areas under the spectra in the 280–310 eV region versus the 345–354 eV region (Figure 1a). I_C/Ic_a ratios measured on different calcium-bearing reference samples with known elemental compositions showed a good correlation with C/Ca molar ratios (R^2 ~ 0.95) (Figure 1b). The reference compounds included carbonate minerals (amorphous calcium carbonate, aragonite, benstonite, calcite, dolomite), calcium-phosphate minerals (francolite, hydroxyapatite), and *Escherichia coli* cells, and have already been described elsewhere (Benzerara et al., 2004; Cam et al., 2015; Cosmidis & Benzerara, 2014; Cosmidis, Benzerara, Guyot, et al., 2015; Cosmidis, Benzerara, Nassif, et al., 2015).

I_C/Ic_a ratios were used to distinguish calcium carbonate mineral phases (empirically defined as I_C/Ic_a <3.3) from organic materials with adsorbed Ca^{2+}. The presence of X-ray absorption features at 290.3 eV and around 301.5 eV was furthermore used to discriminate calcium carbonate minerals from organic matter (absorbing in the 285.0–288.7 eV range) (Brandes et al., 2010) (Figure 1a). A more quantitative assessment of carbonates versus organic carbon concentrations was not attempted due to the fact that the intensity of the X-ray absorption signal 290.3 eV (1 s → π^* electronic transitions in carbonate groups) in carbonate minerals depends on the orientation of the crystals with respect to the X-ray beam (Metzler et al., 2008).

2.4.3 | Determination of calcium carbonate crystallinity: Splitting ratios at the Ca $L_{2,3}$-edge

Calcium carbonate mineral phases were identified by comparison with reference spectra at the Ca $L_{2,3}$-edge. The crystallinity of calcium carbonates was furthermore quantified using calculated splitting ratios

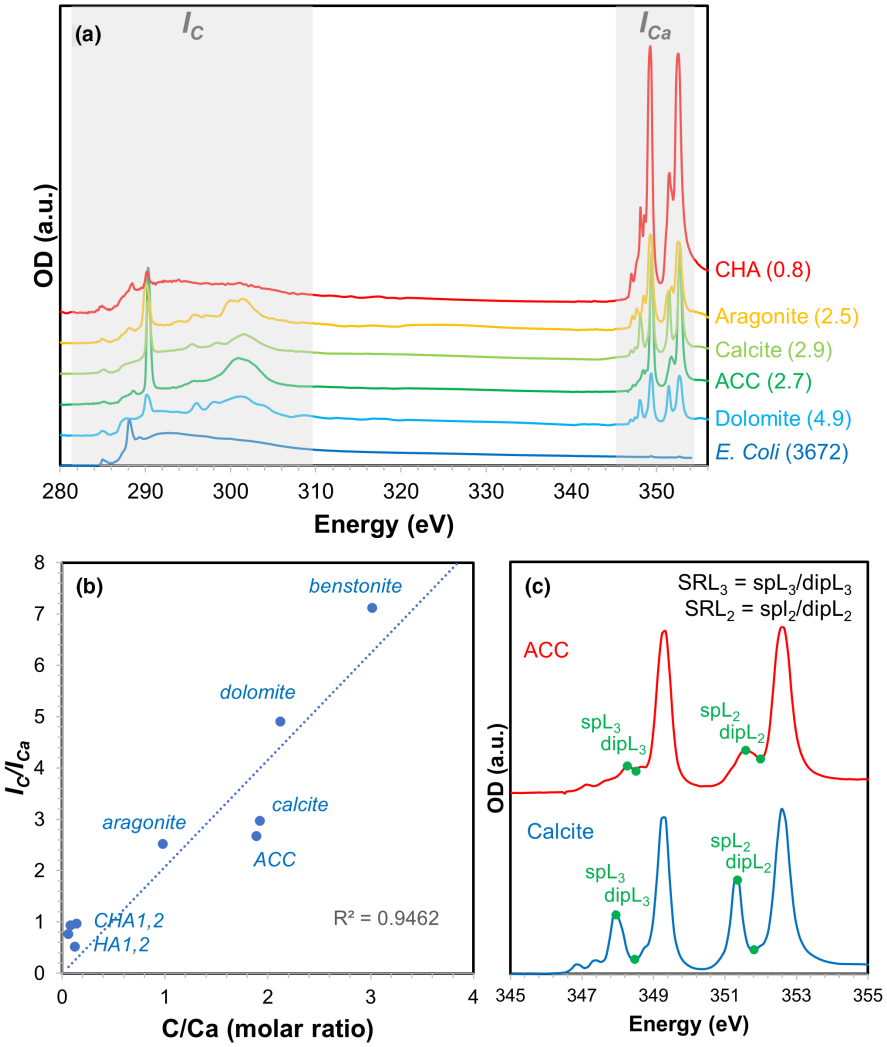

FIGURE 1 STXM methods for the calculation of I_C/I_{Ca} ratios and splitting ratios (SRL_2 and SRL_3). (a) XANES spectra of several reference compounds spanning the C K- and Ca $L_{2,3}$-edges, and calculated I_C/I_{Ca} ratios. I_C/I_{Ca} is calculated as the ratio of the areas under the curve in the 280–310 eV region versus the 345–354 eV region (shaded areas). Calculated I_C/I_{Ca} ratios are noted (numbers in brackets). The C K-edge spectra of carbonate minerals typically display strong absorption peaks at 290.3 eV and broad absorption bands around 301.5 eV. Some of the mineral references contain minor amounts of organics, detectable as small peaks in the 285.0–288.7 eV region. ACC, amorphous calcium carbonate; CHA, carbonated hydroxyapatite (francolite); *E. coli*, *Escherichia coli* cells. (b) Plot showing the correlation between I_C/I_{Ca} ratios and measured C/Ca molar ratios for different calcium-bearing reference minerals. HA, hydroxyapatite. (c) Ca $L_{2,3}$-edge spectra of a reference calcite and amorphous calcium carbonate, showing the method for the calculation of splitting ratios, and quantifying calcium carbonate crystallinity (see Politi et al., 2008)

(SRL_2, SRL_3), which provide a measure of the crystal field splitting at the Ca L_2 and L_3 edges, as defined in Politi et al. (2008). Typically, the Ca $L_{2,3}$-edge spectra of amorphous calcium carbonates (ACC) have poorly split L_2 and L_3 peaks, while the spectra of crystalline phases such as calcite display higher SRL_2 and SRL_3 splitting ratios characteristic of well-resolved split peaks (Politi et al., 2008) (Figure 1c).

3 | RESULTS

3.1 | Geochemical profiles

We recorded vertical physical and geochemical profiles in the top 25 m of the lake water column before (April), during (May–August), and after (September) the 2018 whiting (Figure 2, Figures S1–S2, Tables S1–S6). Temperature profiles (Figure 2) showed a warming of the surface layer of the lake through the spring and summer, starting from an almost vertically linear profile at ~7°C in April, and warming to ~25°C at the surface by August, leading to the development of a thermocline, which moved from a depth of ~3 m in May to ~5 m in September. This thermocline was also reflected in the pH, conductivity, and dissolved oxygen profiles (Figure 2), which showed a more basic, fresher, and more oxygenated wind-mixed surface layer through the season compared with the lower mixolimnion. Below the thermocline, an increase in dissolved oxygen was observed from April to September, likely indicative of summertime primary productivity (oxygenic photosynthesis). These seasonal changes are consistent with past studies of FGL (e.g., Havig et al., 2015; Takahashi et al., 1968).

Variation in calcite saturation state through the FGL whiting was estimated using pH and alkalinity measurements (Figure 2) to constrain the carbonate chemistry, and supplemented with [Ca^{2+}] and other major ion concentrations from June and September (Figure 2, Figure S1). Surface water pH remained fairly stable at ~7.8 throughout the spring and summer and decreased with depth to reach ~6.5–7.3 at the base of the mixolimnion. This pH gradient with depth became steeper through the whiting season, with minimum pH values of ~6.5 achieved below the thermocline in August. Enhanced acidity in the late summer likely recorded cumulative respiration, as reflected in the significantly calculated buildup of CO_2 below ~5 m depth from May to August (Figure 2). Alkalinity profiles were remarkably invariant in time, showing relatively low alkalinity

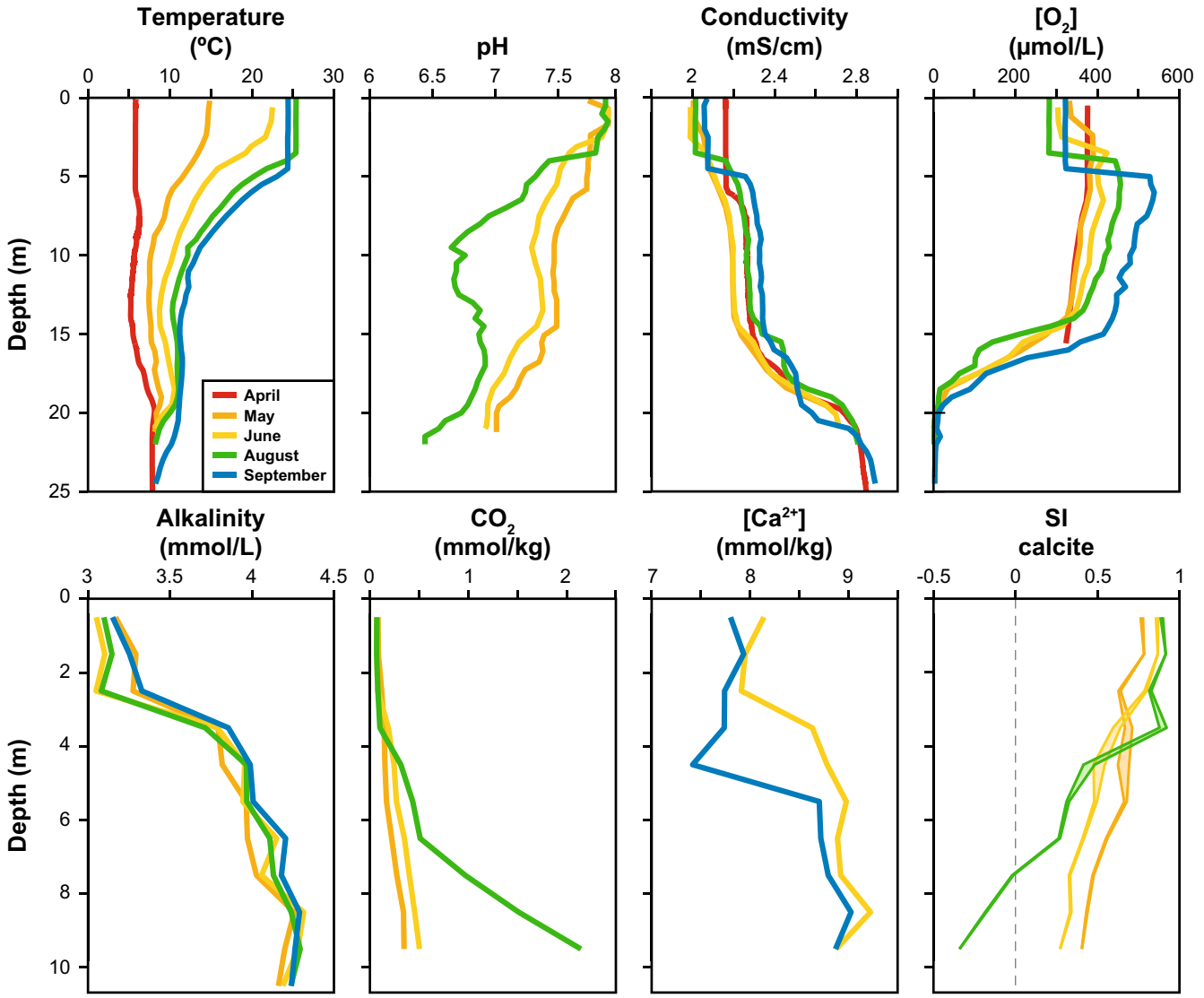

FIGURE 2 Vertical profiles of temperature, pH, conductivity, dissolved oxygen ($[O_2]$), alkalinity, dissolved carbon dioxide (CO_2), calcium ion concentration ($[Ca^{2+}]$), and calcite saturation index (SI) in the FGL water column throughout the 2018 field season (April—Red, May—Orange, June—Yellow, August—Green, September—blue). pH measurements could not be performed in April and September, preventing calculations of dissolved CO_2, DIC, and calcite saturation index. Bounding lines in the calcite SI plot illustrate the sensitivity of the calculated calcite saturation state when using either June or September calcium and other major ion data.

values above the thermocline (~3–3.4 mmol.L^{-1}) and increasing values with depth (to >4 mmol.L^{-1}). Calcium ion concentrations generally increased slightly with depth from ~8 to 9 mmol L^{-1}, although September concentrations are significantly lower than June in the depth range of 3–5 m. The calculated saturation index with respect to calcite (Figure 2) slightly increased above the thermocline through the spring and summer and reached ~1 (10 times supersaturated) at 4 m depth in August. SI generally decreased with depth, and in August FGL became undersaturated (SI <0) below 7–8 m. This trend likely resulted from the CO_2 buildup driven by respiration in the mid-to-late summer, also reflected in the aforementioned August pH gradient.

The redoxcline separating the oxygenated mixolimnion from the euxinic monimolimnion of the lake at ~20 m was marked by a sharp peak in turbidity (Figure S2), corresponding to the "microbial plate" formed by dense populations of photosynthetic sulfur bacteria (Havig et al., 2015; Zerkle et al., 2010). Although whitings at FGL have been reported to cause changes in the clarity of the lake surface waters as measured in changes in Secchi depth (Schultze-Lam et al., 1997), $CaCO_3$ precipitation was not registered on the turbidity profiles.

3.2 | Types and abundances of whiting particles

Particles collected on filters in the FGL water column throughout the whiting season and observed with SEM primarily consisted of centric and pennate diatoms, carbonate minerals grains, microbial cells, and

extracellular organic materials (Figure 3, Figure S3). Calcium carbonate minerals were not visible in SEM images in April but were present in June, with the highest abundances in the 3 m sample, demonstrating the shallow location of the whiting in the water column (Figure 4). Carbonate mineral abundances peaked in the samples in August at 4 m depth. Centric diatoms were the most abundant diatom type and peaked in June at 8 m depth. Both calcium carbonate minerals and diatoms abundances peaked deeper in the water column through the spring and summer (Figure 4).

The surface appearance of carbonate minerals changed through time (Figure 3a–c): Early carbonate grains (June) appeared smooth, while later, carbonate grains (August) developed pitted, rough outer surfaces, and rounder shapes. However, the average size of suspended carbonate grains remained relatively constant with time (~5–7 μm in length) through the whiting. Abundances of microbial cells were not quantified; although visible on SEM images (in particular spherical cells, which may correspond to coccoid picocyanobacteria, see arrows in Figure 3) (Kamennaya et al., 2020; Schultze-Lam et al., 1997), microbes were often obscured by diatoms and carbonate grains due to their small sizes. Carbonate grains and diatoms were found within a mesh of long organic filaments, ~15–100 nm thick. These filaments were also observed aggregated with carbonates and diatoms in sediment trap samples collected at 13 m depth in July 2017 (Figure 3f, Figure S4).

3.3 | Calcium carbonate mineralogy and calcium association with cells and organics

3.3.1 | Prewhiting samples from the FGL water column (April)

Samples collected from the FGL water column at 8 m depth in April 2018 (before the onset of conspicuous calcium carbonate precipitation) were analyzed using STXM at the C K- and Ca $L_{2,3}$-edges (Figures 5–8, Figure S5). Abundant centric diatoms were observed along with spherical and rod-shaped microbial cells (Figure 5). The spherical cells were relatively small (~0.8 μm in diameter), and may correspond to cyanobacteria of the genus *Synechococcus* based on morphology and size. *Synechococcus* is indeed the dominant autotroph in FGL (Schultze-Lam et al., 1997; Thompson et al., 1990) and the only cyanobacterial genus detected in the top part of the water column in recent 16 S rRNA analyses (Kamennaya et al., 2020). Diatoms and bacteria were found amidst extracellular organic material, forming either filaments or thin films (Figures 5–7), and interpreted as EPS produced by microbial cells and/or diatoms. In some images (e.g., Figures 6a, 7a), filamentous EPS clearly radiated from the sides of diatom frustules, strongly suggesting that diatoms were the producers of such EPS. Note that EPS material, although visible on STXM transmission images, did not always appear on organic

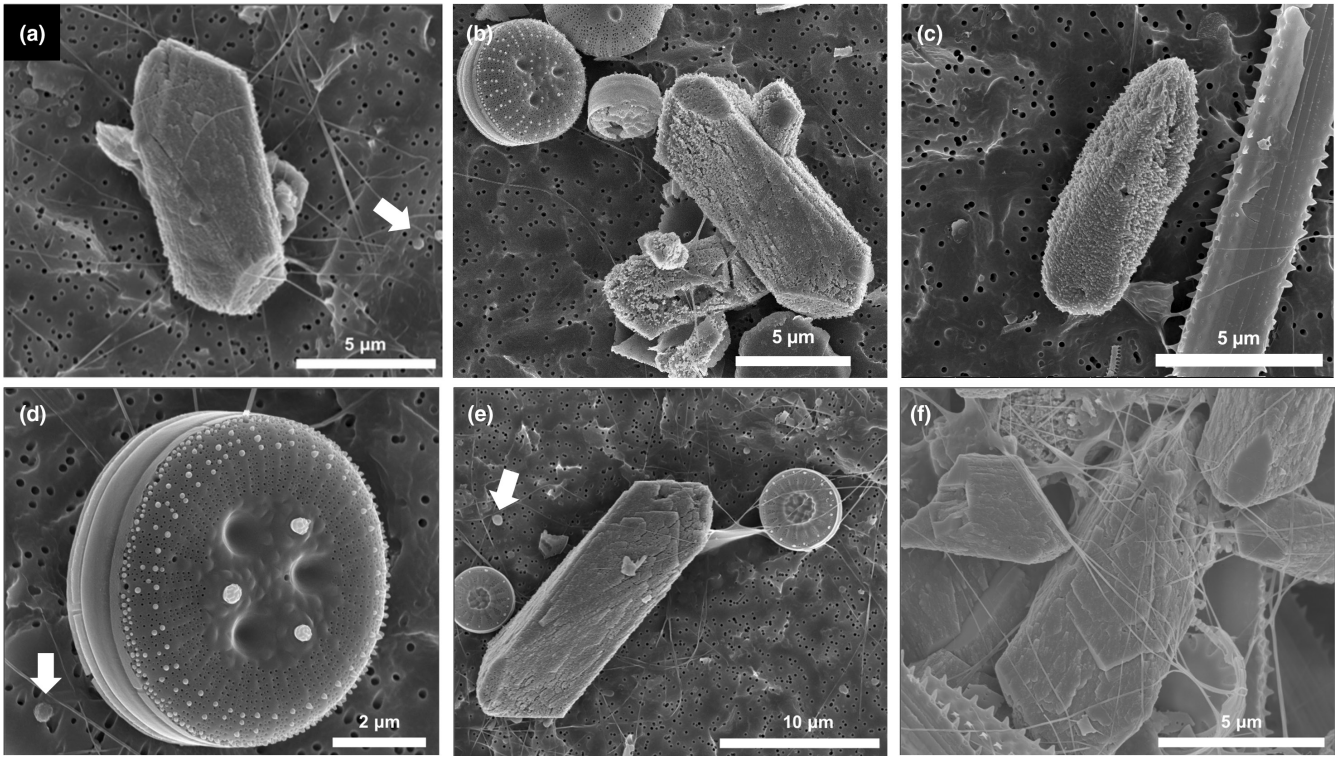

FIGURE 3 SEM images of whiting particles from the FGL water column. (a) Smooth-surfaced calcium carbonate mineral interlaid with organic fibrils, characteristic of early whiting (3 m depth, June). (b) Pitted calcium carbonate grains and centric diatoms (8 m depth, August). (c) Increasingly pitted and rounded carbonate grain, along with pennate diatom (8 m depth, September 8). (d) A centric diatom with organic material (EPS) extruding from the valve pores (3 m depth, June 30). (e) A centric diatom attached to a carbonate mineral grain with organic filame (3 m depth, June). (f) Sediment trap whiting material (July 2017, 13 m depth) showing carbonate minerals within a dense mesh of organic filaments. White arrows point to spherical microbial cells.

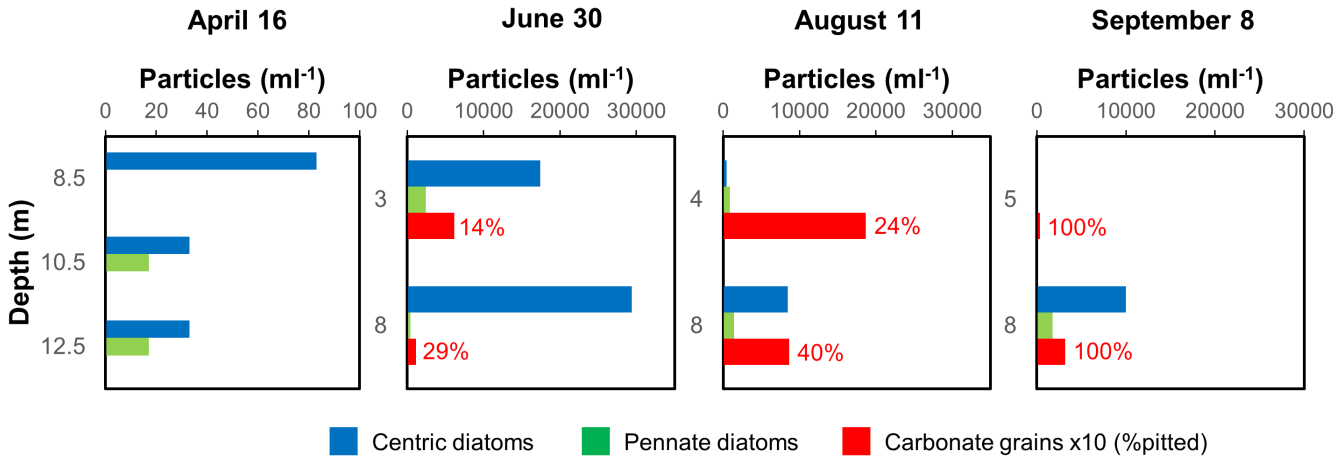

FIGURE 4 Particle types and abundances at different depths in the water column of FGL before and throughout the whiting season, as counted from SEM images. Note that abundances of carbonate grains have been multiplied by ten, and that sample collection depth varies for different sampling times. The percentage of pitted carbonate particles (relative to smooth grains) is indicated.

carbon maps, likely due to their extreme thinness (possibly 10 nm or thinner; Svetličić et al., 2013), which might have prevented the obtention of a proper focus of the X-ray beam and good absorption signal.

C K-edge XANES spectra obtained on spherical microbial cells exhibited a main peak at 288.2 eV (amide groups in peptides), with smaller peaks at 285.0–285.5 eV (aromatics and unsaturated carbon), and shoulders at 286.6 eV (ketonic and phenolic groups), 287.4 eV (aliphatics, phenols and/or ketones), 288.5 eV (carboxylic groups), 289.4 eV (hydroxyl groups, ethers, and/or C=O groups in nucleic acids), and 290.3 eV (carbonate groups) matching previously published bacterial spectra (e.g, Benzerara et al., 2004; Chan et al., 2011; Cosmidis, Benzerara, Nassif, et al., 2015) (Figure 6). In contrast, the C K-edge spectra of the EPS showed a main peak at 288.5 eV (carboxylic groups), consistent with a composition dominated by acidic polysaccharides (Chan et al., 2009; Lawrence et al., 2003; Mitsunobu et al., 2014), with smaller peaks and shoulders around 285.0–285.5 eV (aromatics and unsaturated carbon), 287.4 eV (aliphatics, phenols and/or ketones), 288.2 eV (amide groups), and 289.4 eV (hydroxyl groups, ethers, and/or C=O groups in nucleic acids). Note that peaks at 288.5 and 289.4 eV are also consistent with the presence of β-chitin (Lehmann et al., 2009), which composes the EPS fibrils extruded by many centric diatoms (Gügi et al., 2015; Herth & Barthlott, 1979; Novis et al., 2017).

At the Ca $L_{2,3}$-edge, STXM showed the presence of abundant calcium on EPS films and diatoms, in particular on perforations of the frustules, from which EPS are typically exuded (Herth & Barthlott, 1979) (Figure 7). Relatively minor amounts of calcium were detected on microbial cells (see calcium maps in Figure 5), where this element was only present as adsorbed Ca^{2+}, identifiable by a weak absorption signal at the Ca $L_{2,3}$-edge ($I_{C/Ca}$ ratios 10–50) and absence of strong peaks at 290.3 eV and 301.5 eV (corresponding to carbonates) at the C K-edge. The surfaces of some spherical microbial cells were enriched in adsorbed calcium compared with their interiors, which could be determined by comparing the intensity of the absorption signal at the C K-edge and Ca $L_{2,3}$-edge on the XANES spectra extracted from a cell interior (labeled S1) and cell surface (labeled L) on Figure 8. For instance, for the cell in Figure 8a, $I_C/I_{Ca} = 46$ on the cell interior and $I_C/I_{Ca} = 17$ on the cell surface. The calcium enrichment of the cell surface may be indicative of Ca^{2+} adsorption on surface EPS or S-layers, as described in previous studies (Schultze-Lam et al., 1992; Thompson & Ferris, 1990).

Calcium was furthermore enriched on EPS films, forming irregularly shaped dense clots (white arrows in Figure 5), displaying low I_C/I_{Ca} ratios ranging from 0.5 to 2.5, as well as intense absorptions at 290.3 eV and ~301.5 eV, and thus interpreted as calcium carbonate minerals. At the Ca $L_{2,3}$-edge, their calculated splitting ratios were SRL_3 ~ 1.2–1.4 and SRL_2 ~ 1.3–1.4, matching a reference amorphous calcium carbonate (ACC) (Figure 9). ACC in the prewhiting samples was also found as small (<500 nm) mineral grains located on or nearby spherical microbial cells (phases mapped in blue in Figure 8).

Calcium was finally concentrated in round-shaped areas within the EPS films, measuring ~1 μm in diameter (open arrows in Figure 5d,f). Due to their weak signal at the Ca $L_{2,3}$-edge as compared with ACC grains described above, they likely correspond to adsorbed Ca^{2+} on organic material rather than to calcium carbonate minerals. No XANES spectra were acquired on these objects, preventing calculations of I_C/I_{Ca} ratios.

3.3.2 | Whiting sample (sediment trap)

STXM analyses were performed on whiting particles collected in a sediment trap placed in the FGL water column at 13.5 m depth between July 12 and July 21, 2017 (Figure 10, Figure S6). The sample contained abundant calcium carbonate particles, measuring up to 7 μm in length, and identified as calcite based on Ca $L_{2,3}$-edge

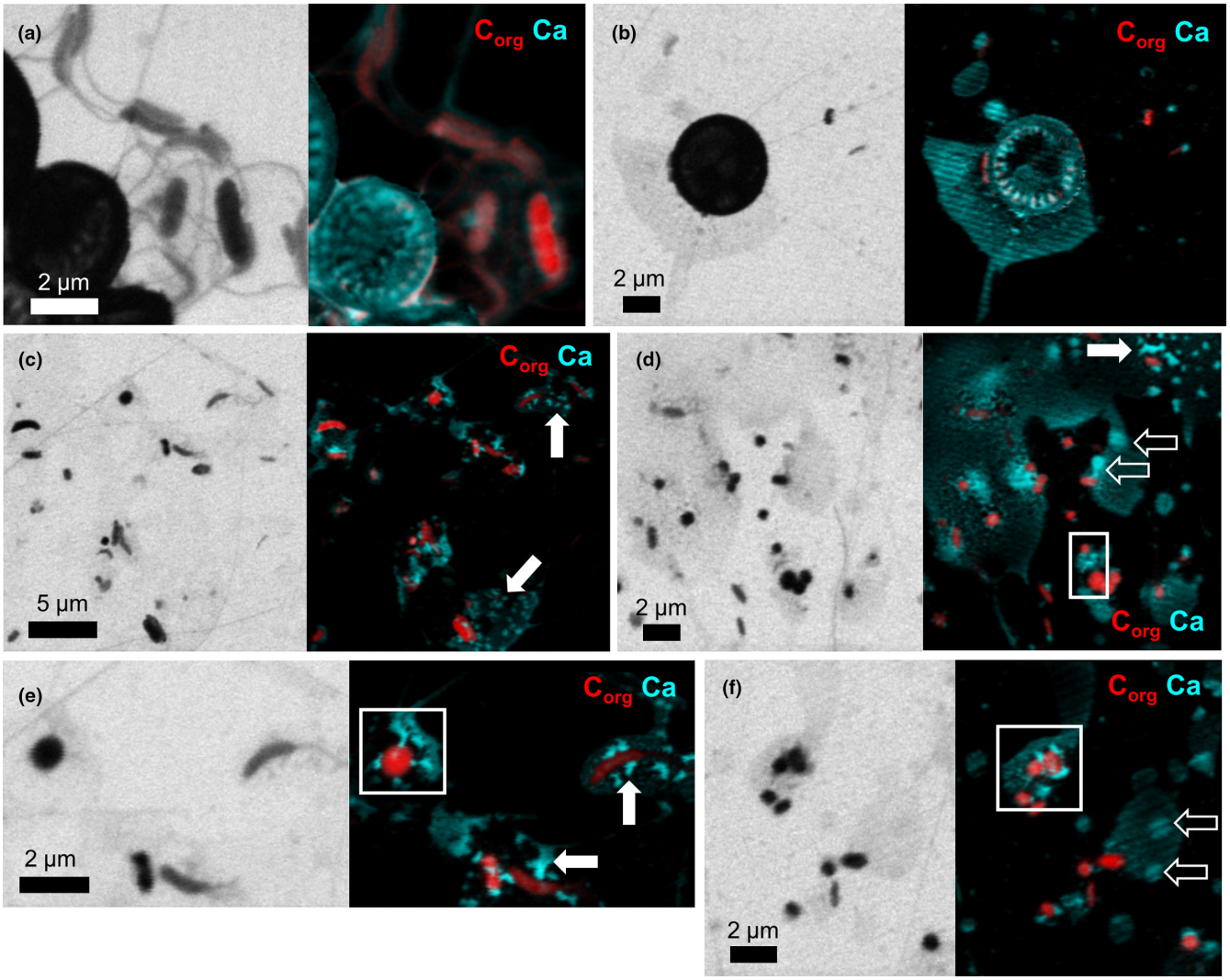

FIGURE 5 STXM analyses of prewhiting particles from the FGL water column (April, 8 m depth). Images (left) were acquired at 288.2 eV. The corresponding maps (right) show the distribution of organic carbon (red) and calcium (cyan). White squares show the locations of the image stacks displayed in Figure 8. White arrows show the location of irregularly shaped calcium-rich clots within EPS films identified as ACC minerals, while open arrows show micron-sized, round calcium enrichments. Note that EPS films and filaments visible on STXM images do not appear on organic carbon maps, which may be due to their small thickness.

XANES spectra, in agreement with previous studies of whitings at FGL (Schultze-Lam et al., 1997; Thompson et al., 1990). Calculated I_C/I_{Ca} ratios for these calcite grains ranged between 2.5 and 3.3, and splitting ratios at the Ca $L_{2,3}$-edge were $SRL_2 \sim 1.6–1.7$ and $SRL_3 \sim 1.8–2.0$ (Figure 8), consistent with crystalline calcite (Politi et al., 2008). C K-edge XANES spectra obtained on the calcite grains sometimes displayed absorption peaks at 288.2–288.5 eV (amides and carboxylics), suggesting that organic compounds may be adsorbed onto or incorporated within the mineral particles (Figure 10d).

The calcite grains were forming aggregates also containing centric diatoms and organic material, present either as filaments or as organic particles surrounding the minerals. Microbial cells were not observed in the sediment trap sample. The C K-edge XANES spectra of the organic filaments and particles displayed main peaks at 288.5 eV (carboxylic groups) and 288.2 eV (amide groups), with smaller peaks or shoulders at 285.0 and 285.5 eV (aromatics and unsaturated carbon), 286.6 eV (ketonic and phenolic groups), 287.4 eV (aliphatics, phenols and/or ketones), 289.4 eV (hydroxyl groups, ethers, and/or C=O groups in nucleic acids). This composition was similar to that of EPS films and filaments previously described in prewhiting samples from the water column, with an increased contribution from amide groups, which may be derived from proteins issued from decomposing microbial cells. The organic filaments and particles displayed high I_C/I_{ca} ratios (73–605) and no absorption signal from carbonates at the C K-edge, showing that calcium was only present as minor amounts of adsorbed Ca^{2+}. Similarly, the diatoms displayed C K-edge XANES spectra consistent with cellular material with main absorption features characteristic of amides and carboxylic groups and absence of strong carbonate signal, with relatively high I_C/I_{ca} ratios (e.g., $I_C/I_{ca} = 61$ for the diatom fragment in Figure S6) consistent with the presence of adsorbed Ca^{2+} only.

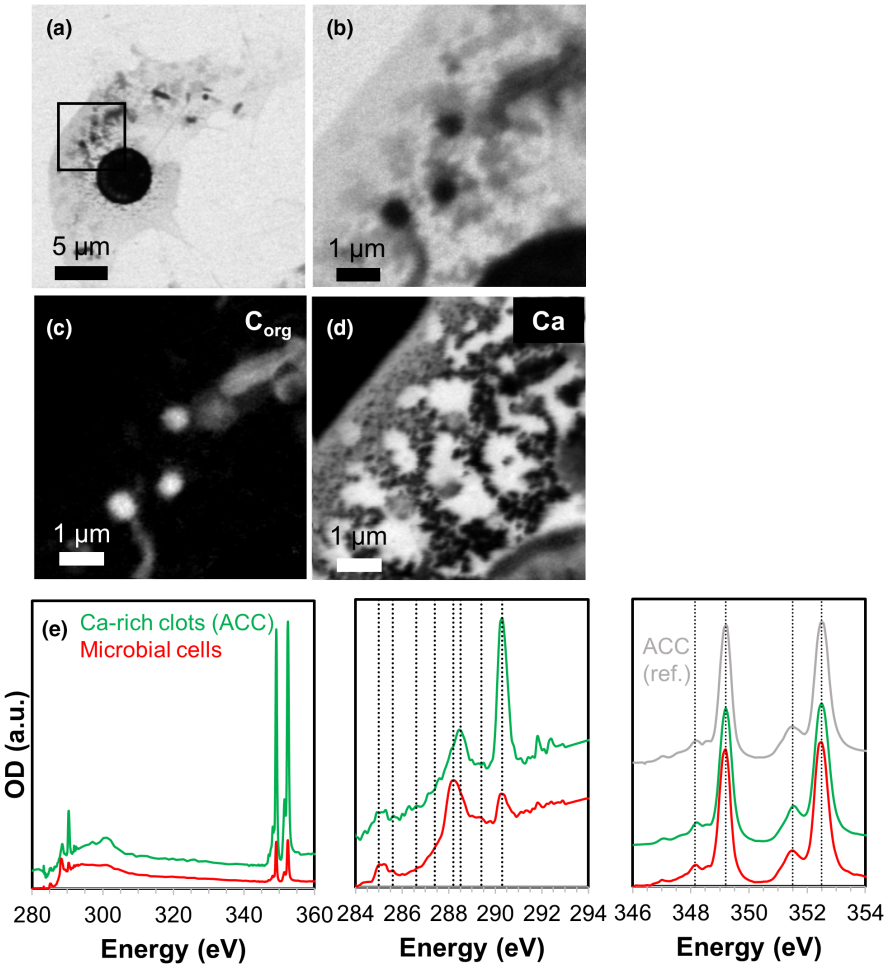

FIGURE 6 STXM analyses of diatom EPS and microbial cells from an FGL pre-whiting sample (April, 8 m depth). (a) Image obtained at 288.2 eV. A centric diatom, surrounded by EPS film, is visible. (b) Close-up on the area depicted by a square in (a). Spherical microbial cells are present within the EPS film. (c) Organic carbon map. (d) Calcium map. (e) XANES spectra are representative of calcium-rich clots within the EPS film (green) and microbial cells (red). C K-edge spectra (middle panel): Vertical lines correspond to the absorption energies of different functional groups (see main text). Ca $L_{2,3}$-edge spectra (right panel): Vertical lines correspond to the position of the main peaks in the reference amorphous calcium carbonate (ACC) spectrum (gray). The calcium-rich clots were identified as calcium carbonate phases based on the presence of strong X-ray absorption at 290.3 eV and 301.5 eV. Their calculated splitting ratios were $SRL_3 \sim 1.2$ and $SRL_2 \sim 1.3$, corresponding to ACC.

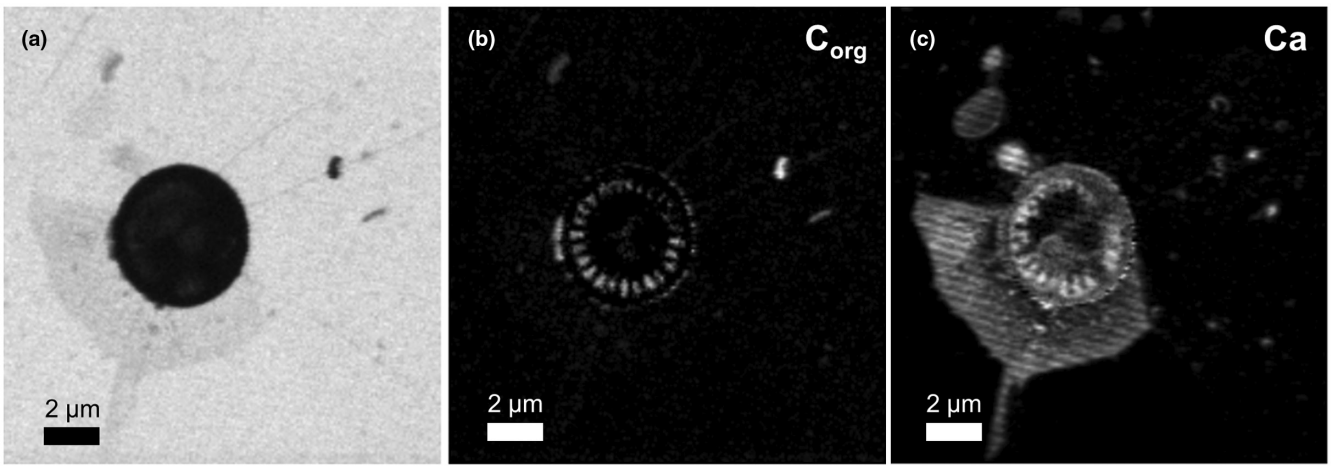

FIGURE 7 STXM image and maps of a centric diatom and associated EPS in an FGL prewhiting sample (April, 8 m depth). (a) Image at 288.2 eV. (b) Organic carbon map. (c) Calcium map. Calcium is particularly enriched on the EPS material around the diatom and on the perforations of the frustule (from which EPS are typically exuded).

3.3.3 | Sediment core samples

STXM analyses of sediment core samples from the bottom of FGL are presented in Figure 11, as well as Figures S7 and S8. The sediment contained abundant calcium carbonate grains, identified as calcite based on their Ca $L_{2,3}$-edge spectroscopic signature, and similar in shape and size to those observed in the whiting samples. I_C/I_{Ca} ratios measured on the sediment calcite particles ranged between 2.1 and 2.6, and splitting ratios at Ca $L_{2,3}$-edges were $SRL_3 \sim 1.9–3.2$ and $SRL_2 \sim 1.8$ and 2.2 (SRL_2) (Figure 9), indicating increased crystallinity

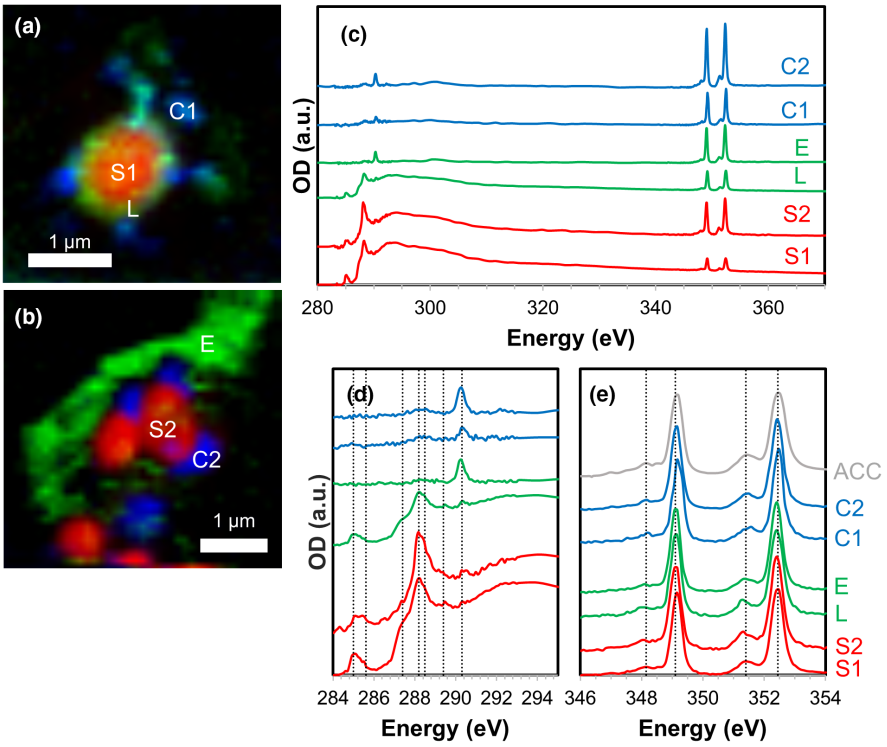

FIGURE 8 STXM analyses of spherical microbial cells, EPS, and calcium-rich grains in an FGL prewhiting sample (April, 8 m depth). (a) and (b): Maps showing the distribution of different components extracted from image stacks. S1, S2: Spherical cells; L: Outer layer of a cell; E: EPS; C1, C2: Calcium-rich grains. (c) Corresponding XANES spectra spanning the C K- and Ca $L_{2,3}$-edges. (d) C K-edge XANES spectra normalized at 320 eV. Vertical lines correspond to energy positions of the main absorption features of different function groups (see main text). (e) Ca $L_{2,3}$-edge spectra, normalized at 349.2 eV (energy of the Ca L_3 peak). Vertical lines correspond to the energy positions of the main absorption features of amorphous calcium carbonate (ACC). Both the calcium-rich grains (C1, C2) and EPS (E) have spectroscopic signatures consistent with ACC.

compared with the whiting calcite particles from the sediment trap. C K-edge XANES spectra obtained on these sedimentary calcite particles displayed peaks at 288.2–288.5 eV, again showing possible adsorption or incorporation of organic molecules.

Calcite grains occurred aggregated with abundant diatom frustules, which were sometimes fragmented. Diatoms were mostly centric, with fewer pennate forms (e.g., Figure 11c, Figure S7). The diatoms were associated with higher amounts of calcium compared with diatoms from the sediment trap, as visible on STXM calcium maps (Figure 11, Figures S7a and S8a). This abundance of calcium was reflected in low I_C/I_{Ca} ratios ranging from 3.4 to 7.5. Combined with strong absorption signals at 290.3 eV at the C K-edge (see in particular Figure S8b), low I_C/I_{Ca} ratios indicated the presence of fine calcium carbonate phases associated with the diatoms frustules. Calculated splitting ratios at the Ca $L_{2,3}$-edge ranged between those of ACC and calcite (SRL_2 ~ 1.3–1.6 and SRL_3 ~ 1.1–1.5), corresponding to either ACC or poorly crystalline calcite.

Organic matter in the sediment samples was found in diatoms and rare extracellular filaments (Figure S7), as well as dense organic-rich particles found around diatoms and calcite grains, measuring up to ~5 µm (see arrow in Figure S8). These organic particles had C K-edge signatures similar to that of organic particles in the sediment traps.

4 | DISCUSSION

4.1 | Biogeochemical processes at the origin of the FGL whiting

Calcium carbonate precipitation in low-temperature aqueous environments may generally occur as a result of environmental or biological processes impacting the calcium carbonate saturation index (the "alkalinity engine") and/or under the influence of organic surfaces such as cells and EPS, which can provide a template for carbonate nucleation (Dupraz et al., 2009). Comparing the timing and location of calcite precipitation with observed geochemical changes in the water column can allow us to shed light on the respective importance of these different processes in whiting events (Broecker & Takahashi, 1966; Long et al., 2017; Robbins & Blackwelder, 1992).

In our study, conspicuous calcite crystals were first observed at ~3 m depth in June and peaked at ~4 m depth in August (Figure 4), coinciding with a peak in calcite saturation index that month (~0.9 at 3.5 m) (Figure 2). Sampling at higher spatial and temporal resolutions performed by Schultze-Lam et al. (1997) painted a more complex picture of the FGL whiting, with calcite abundances peaking twice through the spring and summer. A first peak was indeed

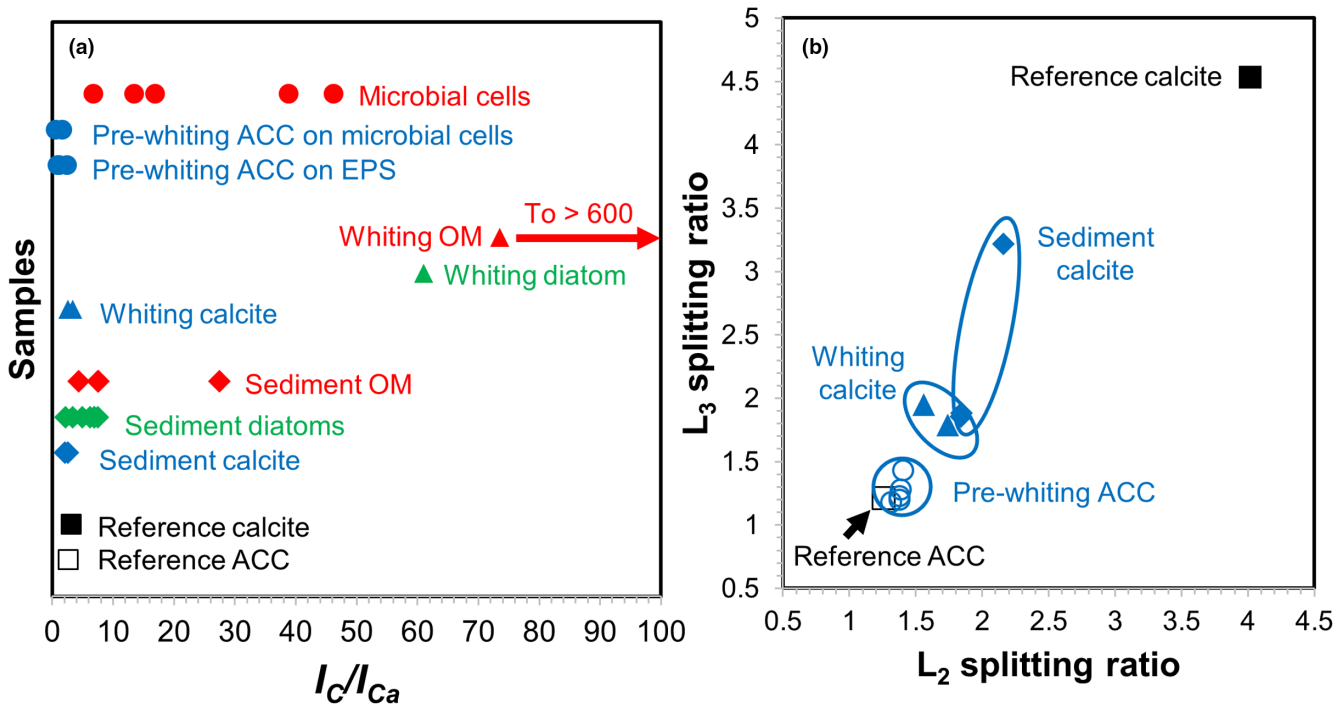

FIGURE 9 I_C/I_{Ca} ratios and splitting ratios (SRL_3, SRL_2) for different types of samples from the FGL water column and sediment. Ratios calculated from reference spectra for calcite and amorphous calcium carbonate (ACC) were also plotted for comparison. (a) I_C/I_{Ca} ratios: Prewhiting microbial cells and ACC correspond to the water column sample collected in April at 8 m depth. Whiting calcite, diatoms, and organic matter (OM) correspond to sediment trap samples (July, 13.5 m depth). Note that sediment trap OM I_C/I_{Ca} values ranged from ~73 to >600 (off chart). Sediment calcite, diatoms, and OM correspond to sediment core samples. (b) SRL_3 versus SRL_2 plot for calcium carbonate particles from the pre-whiting water column (April, 8 m depth) (pre-whiting ACC), the sediment trap (whiting calcite), and the sediment core (sediment calcite). Only particles with I_C/I_{Ca} ratios smaller than 3.3, identified as calcium carbonate minerals, were plotted on this chart.

observed in May–June, with high calcite abundances at both 4 m and 8 m depths, followed by a second, smaller peak in August, mostly occurring at 8 m depth. It is possible that the pattern and timing of the whiting vary from year to year based for instance on climatic variability.

An obvious abiotic factor that may be driving high calcite saturation (>0.75) and precipitation at FGL in the spring and summer is the significant warming of the surface of the lake (from ~5°C in April to ~25°C in August) (Figure 2), with peak temperatures coinciding with observed peak $CaCO_3$ precipitation at ~4 m depth in August. However, previous studies at FGL have proposed a biological whiting mechanism based on photosynthetically driven alkalization (Schultze-Lam et al., 1997). In their analysis of the SW Florida whiting, Long et al. (2017) explained that an entirely abiotic $CaCO_3$ precipitation mechanism would be accompanied by a decrease in alkalinity and pH and an increase in CO_2, whereas a biologically induced mechanism would not lead to changes in carbonate parameters due to counterbalancing effect of photosynthesis on $CaCO_3$ precipitation. In the present study, alkalinity stayed remarkably stable around ~4 m depth (where peak calcite precipitation is thought to occur) from May to September. pH and CO_2 concentrations also stayed relatively constant at this depth through the duration of the whiting. Below 4 m, a pH decrease accompanied by an increase in CO_2 concentrations was observed from May to August, but this trend was most likely driven by respiration processes rather than abiotic $CaCO_3$ precipitation, since maximum CO_2 concentrations (below ~7 m depth in August) occurred deeper in the water column as compared to $CaCO_3$ formation (~4 m depth; Figures 2 and 4). Our geochemical measurements thus support an important role of photosynthetic activity in $CaCO_3$ precipitation at FGL, in agreement with previous studies (Schultze-Lam et al., 1997), although surface warming of the water column is likely to be a reinforcing abiotic factor.

Photosynthetic intensities may be visualized on dissolved oxygen profiles recorded in the FGL mixolimnion (Figure 2). Oxygen concentrations, at equilibrium with the atmosphere in the top wind-mixed layer of the lake, were observed to increase abruptly at the top of the thermocline from May to September, reflecting photosynthetic oxygen production during the spring and summer. Photosynthesis in the top mixolimnion of FGL is thought to be driven by cyanobacteria of the genus *Synechococcus*, as well as diatoms (Kamennaya et al., 2020; Thompson et al., 1990). According to Schultze-Lam et al. (1997), *Synechococcus* is the main biological agent photosynthetically driving $CaCO_3$ precipitation at Green Lake, based on the fact that *Synechococcus* were observed by these authors to outnumber diatoms by up to five orders of magnitude in the upper mixolimnion. However, it has to be noted that in their study, maximum abundances of *Synnechococus* were not spatially and

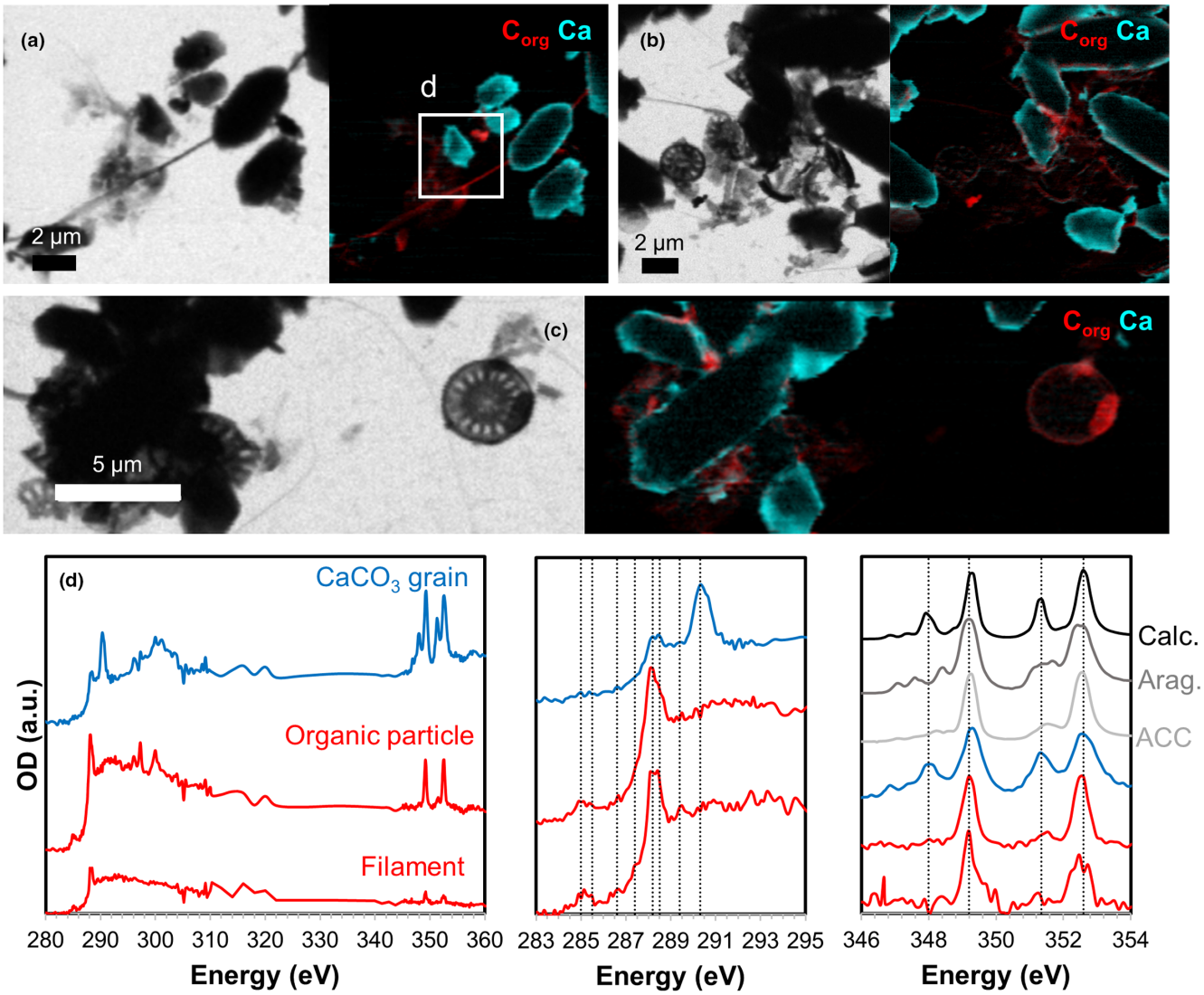

FIGURE 10 STXM analyses of settling whiting particles collected in a sediment trap (July 2017, 13.5 m depth). (a-c) Images at 288.2 eV (left) and maps of organic carbon (red) and calcium (cyan) (right). The interior of $CaCO_3$ grains sometimes appeared black on calcium maps due to the excessive thickness of the grains, causing saturation of the X-ray absorption signal. The white box in (a) represents the location of the image stack from which spectra shown in (d) were extracted. (d) XANES spectra representative of a $CaCO_3$ grain, an organic filament, and a dense organic carbon particle in (a). C K-edge spectra (middle panel): Vertical lines correspond to the absorption energies of different functional groups (see main text). Ca $L_{2,3}$-edge spectra (right panel): Vertical lines correspond to the position of the main peaks in a reference calcite (calc.) spectrum (black). Reference Ca $L_{2,3}$-edge XANES spectra for aragonite (Arag.) and amorphous calcium carbonate (ACC) are also shown.

temporally correlated with maximum calcite abundances (Schultze-Lam et al., 1997), which seems in contradiction with their model. Unfortunately, *Synechococcus* abundances were not determined in our own study. We can, however, note that our measured diatom abundances did not correlate with calcite abundances (Figure 4), suggesting that the photosynthetic activities of diatoms were not mainly driving $CaCO_3$ precipitation. The relative photosynthetic contributions of cyanobacteria and diatoms in the upper water column of FGL may be determined in future studies, employing for instance pigment analyses of sequencing data (e.g., Fulton et al., 2018; Rojas et al., 2021).

4.2 | Organic-mineral interactions during the FGL whiting

In addition to the photosynthetically driven "alkalinity engine" discussed in the previous section, our observations suggest that organic-mineral interactions involving microbial cells and EPS likely play an important role in calcium carbonate mineralization at the onset of the FGL whiting. In April, STXM analyses revealed fine ACC phases covering abundant EPS, often radiating from diatoms (Figures 6–7), as well as microbial cells (possibly corresponding to *Synechococcus* based on previous studies; Thompson

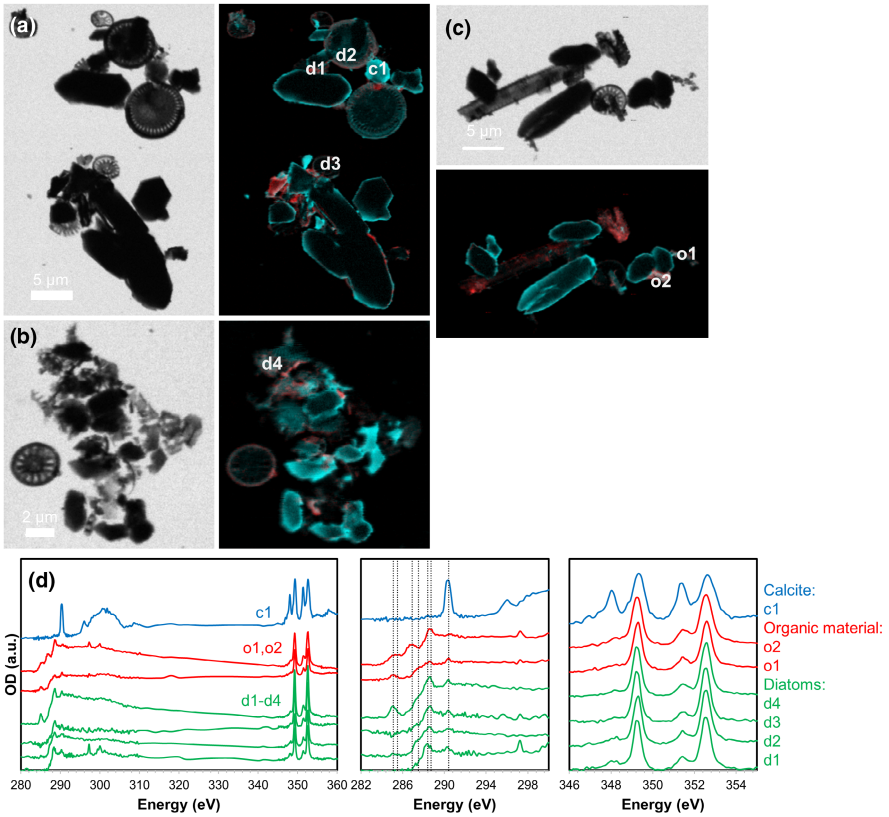

FIGURE 11 STXM analyses of particles from an FGL sediment core at 0–2 inches (a, b) and 2–4 inches (c) depths below the lake floor. (a–c) Images at 288.2 eV (left) and maps of organic carbon (red) and calcium (cyan) (right). The locations from which XANES spectra shown in (d) were extracted are indicated: c1 (calcite grain), o1-o2 (organic material), and d1-d4 (diatoms). (d) Corresponding XANES spectra. C K-edge spectra (middle panel): Vertical lines correspond to the absorption energies of different functional groups (see main text). Right panel: Ca $L_{2,3}$-edge spectra

& Ferris, 1990; Schultze-Lam et al., 1992, 1997) (Figure 8). The precipitation of ACC minerals was likely facilitated by the adsorption of Ca^{2+} on organic surfaces such as microbial cells, diatoms, and EPS including materials exuded from the apertures of the silica valves (Figures 5–8). Concentration of Ca^{2+} on round-shaped objects ~1 µm in diameter (open arrows in Figure 5d,f) may furthermore correspond to "bag-like" EPS envelopes issued from *Synechococcus* cells, which can dissociate from the cells and have high Ca^{2+} adsorption capacity (Kamennaya et al., 2020). At the molecular level, adsorption of Ca^{2+} ions can occur on negatively charged functional groups such as deprotonated carboxylic groups in acidic polysaccharides and proteins. In FGL waters, at pH 6–8, carboxyl groups exist in a deprotonated state (Beveridge, 1981), and photosynthetic CO_2 uptake may result in local pH increases surrounding cyanobacteria and diatoms, further facilitating deprotonation and calcium binding.

A significant portion of the abundant EPS found associated with calcite particles later in the summer (July; Figure 3, Figure S4) occurred as filaments. These filaments were already observed radiating from diatoms in earlier samples (Figures 3d and 7a). Based on the thickness and C K-edge XANES composition, they may correspond to β-chitin fibrils (Gügi et al., 2015; Herth & Barthlott, 1979; Novis et al., 2017). Indeed, many centric diatoms from the *Cyclotella* and *Thalassiosira* genera excrete β-chitin fibrils through specialized pores of the thecae called fultoportulae (Brunner et al., 2009; Durkin et al., 2009; Gügi et al., 2015; LeDuff & Rorrer, 2019). Although the taxonomy of dominant centric diatom species present at FGL could not be formally determined, they likely belong to *Cyclotella* based on morphology (compare for instance Figure 3d with figures 46–49 in Cvetkoska et al., 2014). Chitin is known to play an important role in the control of $CaCO_3$ biomineralization in mollusk shells and some calcifying algae (e.g., Chan et al., 2018; Rahman & Halfar, 2014). Chitin is a biopolymer with a crystalline structure that is composed of parallel or antiparallel chains of poly-N-acetyl-glucosamine. Pure chitin has a poor affinity for calcium (Tokura et al., 1983) due to the absence of ionic binding sites. Indeed, functional groups, which may coordinate cations such as hydroxyl groups (-OH), and acetyl amino groups ($-NHCOCH_3$) (Wei et al., 2021) are engaged in hydrogen bonding in crystalline chitin, making its surface inert. In Eukaryotic biomineralization systems, chitin typically forms a 2D or 3D scaffold for polyanionic polysaccharides or proteins that direct $CaCO_3$ nucleation and growth (Arias & Fernández, 2008; Ehrlich, 2010; Falini & Fermani, 2004), but it is unclear whether chitin fibrils excreted by diatoms are associated with other biomolecules that could bind Ca^{2+} and nucleate $CaCO_3$ (e.g., Durkin et al., 2009), a question that deserves further investigation. However, our STXM analyses clearly showed Ca^{2+} and ACC clots on film-like EPS material surrounding diatoms, as well as abundant calcium adsorbed onto organic material present within the pores of centric diatom frustules in prewhiting samples (Figures 5–7). While the chemical composition of these calcium-binding EPS will have to be determined in future studies, our observations suggest an important role of diatom EPS in $CaCO_3$ nucleation at the onset of the whiting at FGL.

A role of *Synechococcus* S-layers in calcium carbonate nucleation and templating has been proposed in earlier studies (Schultze-Lam

et al., 1992; Thompson & Ferris, 1990), but the implication of diatom EPS in $CaCO_3$ nucleation at FGL is proposed here for the first time. Küchler-Krischun and Kleiner (1990) observed a correlation between spring blooms of algae including centric diatoms (*Stephanodiseus hantzschii*) and calcite precipitation in the surface waters of Lake Constance, and proposed a whiting model based on $CaCO_3$ nucleation on the algal surfaces. More recent studies have described spatial associations of centric diatoms with calcium carbonate precipitates in the water column of Lake Stechlin (Germany) (Fuchs et al., 2016), as well as in a southwest Florida whiting event (Long et al., 2017). In the second example, amorphous and crystalline $CaCO_3$ particles were observed along the diatom girdle bands, which was explained by the unique surface chemistry (possibly, the presence of specific EPS) and chemical microenvironment in this region of the diatom frustule.

Further studies are needed to determine the relative contributions of cyanobacteria and diatoms in triggering $CaCO_3$ nucleation during whiting events. It is possible that whiting nucleation mechanisms at FGL have evolved over time, with varying contributions of cyanobacteria versus diatoms through the lake's recent history. Predominant mechanisms of calcium carbonate nucleation may shift depending on the microbial community dynamics in the water column, as a result of changes in climatic conditions and/or in the nutrient status of the lake.

In the summer, during the peak of the whiting, calcium carbonate is found as crystalline calcite grains, up to ~7 μm in size, aggregating with diatoms, as well as EPS materials including abundant filaments (possibly corresponding to β-chitin fibrils) (Figures 3 and 10). It is unclear whether the whiting calcite particles correspond to the crystallization and growth of ACC particles observed in prewhiting samples, although ACC is a common precursor phase to crystalline calcite in biologically mediated calcification (Weiner et al., 2005), in particular in $CaCO_3$ mineralization on microbial EPS (Enyedi et al., 2020; Shiraishi et al., 2020). Intermediate phases between nano-ACC particles and calcite crystals measuring several micrometers in length were not observed, which may be due to fast calcite growth in supersaturated solutions (see next section below).

In the sediment trap whiting sample (July), organic materials and diatoms associated with the calcite particles display very small amounts of adsorbed Ca^{2+} as compared with prewhiting samples (see high I_C/I_{Ca} values in Figure 9). Low amounts of calcium adsorbed on organics and diatoms in this whiting sample may thus suggest that calcite minerals grew at the expense of Ca^{2+} initially adsorbed on biological materials. Ca^{2+} release from organics and subsequent $CaCO_3$ precipitation may be associated with EPS degradation in the sediment trap, a mechanism that is thought to be important in some calcifying microbial mats (Dupraz & Visscher, 2005). However, it is not clear whether this process is important for the FGL whiting in general (i.e., without detention in a sediment trap), since Ca^{2+}-binding EPS may be rapidly exported out of the shallow waters where $CaCO_3$ precipitation is occurring (top 8 m of the water column; Schultze-Lam et al., 1997).

4.3 | The fate of whiting particles: Calcite growth, partial dissolution, and sedimentation

The end of the whiting season is marked by a decline in calcite mineral abundances in the water column in September (Figure 4). Although the surface waters of the lake remained supersaturated with respect to calcite in the late summer (Figure 2; Brunskill, 1969), the termination of the whiting may be linked with the decline in abundances of photosynthesizing organisms in shallow waters with time, leading to a shortage of organic surfaces for calcium carbonate heterogeneous nucleation.

The duration of the whiting is additionally controlled by the settling rate of mineral particles. According to Stokes Law, settling rates of mineral grains increase exponentially with size (e.g., Gibbs et al., 1971). This phenomenon results in a dramatic increase in settling rate as minerals grow longer than 10 μm in length. Ignoring shape effects on settling rate, a spherical calcite grain 5–7 μm in diameter has a Stokes Law settling rate of ~1 m/day in still waters (e.g., Gibbs et al., 1971). Whiting calcite particles likely have somewhat longer residence times in the turbulent mixolimnion than these still-water settling rates imply, and smaller particles likely remain suspended in the upper portion of the lake for longer, contributing to the light scattering by carbonate grains, giving the lake its turquoise color. However, minerals in the mixolimnion likely grow quite fast, up to 2 μm/day, based on saturation state rate studies conducted by Wolthers et al. (2012) and calcite saturation states reported here. Thus, a mineral can quickly grow to 5–7 μm in length over the span of 2–3 days, sinking as it grows. A mineral 1 μm in size at the surface will sink <0.5 m in a day but grow to a size of 3 μm over the same span of time. Small minerals, on the order of <5 μm in size, were not found suspended in the water column, likely because the growth rate of these grains is fast following nucleation on organic templates. Minerals larger than 15 μm were not found suspended in the water column, consistent with their calculated very short residence time. As demonstrated above, calcite particles were furthermore frequently found in aggregates formed by diatom frustules and EPS, which would also increase settling rates. All told, the residence time of a mineral grain in the upper 10 m of the lake is estimated to be less than 7 days when taking into account combined growth and sinking. In order to support the continued growth and settling of mineral grains, nucleation of new minerals must be continuous throughout the duration of the whiting event.

The high abundance of calcite grains in the FGL sediments (Figure 11, Figures S7 and S8) suggests that settling whiting particles reach the bottom of the lake despite some dissolution in the mixolimnion in the late summer (as evidenced by corroded grain surfaces below ~8 m depth in August and September; Figures 3 and 4, Figure S3). The sedimented calcite particles displayed similar shapes and sizes to those found in the water column, but they were slightly more crystalline (Figure 9b). Calcite in the sediments was found in association with diatom frustules and organic materials (including filaments; Figure S7), which could be coated by important amounts of calcium (Figure 9a), possibly reflecting the higher concentrations of

dissolved Ca^{2+} in the lake monimolimnion (Havig et al., 2015). Calcite grains and diatoms were the main components of FGL bottom sediments, suggesting that these sediments record biogeochemical signals (such as carbon isotopic signatures) from the lake surface waters (Havig et al., 2017).

5 | CONCLUSION

In this work, we used a combination of microscopy analyses and geochemical measurements to shed new light on the mechanism of whitings events at Fayetteville Green Lake. Our results suggest that the annual whiting is induced by the photosynthetic activity of cyanobacteria and diatoms, possibly reinforced by the important warming of the surface of the lake in the spring and summer months. Calcite precipitation occurs via nucleation of an amorphous calcium carbonate precursor phase on microbial cell surfaces, as well as on abundant organic substances (EPS) produced diatoms and bacteria. A role of diatoms in whitings at Fayetteville Green Lake is described here for the first time, with the observation of ACC forming on EPS films and filaments surrounding centric diatoms and extruded from pores in their frustules. Calcite particles are found associated with diatoms and organic materials in the lake sediment, which may thus preserve a record of the mineralization processes occurring at the lake surface.

This study feeds into a growing body of literature showing that diatoms may be overlooked players in calcium carbonate formation processes in nature, in particular in the context of whitings (Fuchs et al., 2016; Long et al., 2017) but also in microbialites (e.g., Gomez et al., 2018; Winsborough, 2000). This work also highlights the relevance of high spatial resolution spectromicroscopy approaches such as STXM to improve our understanding of the organic-mineral interactions at play in large-scale mineralization processes in the environment.

ACKNOWLEDGMENTS

This work was funded through the Penn State Energy and Environmental Sustainability Laboratories (EESL) Green Program and Pennsylvania Space Grant Consortium awards to Chloe Stanton. The authors are indebted to the staff at Green Lakes State Park (NY) for their assistance. Karim Benzerara (Sorbonne Université, CNRS) is thanked for sharing XANES reference spectra, and Stephen Romaniello (University of Tennessee, Knoxville) is thanked for providing an FGL sediment trap sample. Jeff Havig, Beth Herndon (University of Minnesota), and Michael McCormick (Hamilton College) are specially thanked for collecting and providing sediment core samples.

Part of the research described in this paper was performed at the Canadian Light Source, a national research facility of the University of Saskatchewan, which is supported by the Canada Foundation for Innovation (CFI), the Natural Sciences and Engineering Research Council (NSERC), the National Research Council (NRC), the Canadian Institutes of Health Research (CIHR), the Government of Saskatchewan, and the University of Saskatchewan. This research used resources from the Advanced Light Source, a U.S. DOE Office of Science User Facility under contract no. DE-AC02-05CH11231.

CONFLICT OF INTEREST

The authors declare no conflict of interest.

DATA AVAILABILITY STATEMENT

The data that support the findings of this study are available from the corresponding author upon request.

ORCID

Julie Cosmidis https://orcid.org/0000-0003-3428-8447

REFERENCES

Arias, J. L., & Fernández, M. S. (2008). Polysaccharides and proteoglycans in calcium carbonate-based biomineralization. *Chemical Reviews*, *108*, 4475–4482.

Bathurst, R. G. C. (1966). Boring algae, micrite envelopes and lithification of molluscan biosparites. *Geological Journal*, *5*, 15–32.

Benzerara, K., Bolzoni, R., Monteil, C., Beyssac, O., Forni, O., Alonso, B., Asta, M. P., & Lefevre, C. (2021). The gammaproteobacterium Achromatium forms intracellular amorphous calcium carbonate and not (crystalline) calcite. *Geobiology*, *19*, 199–213.

Benzerara, K., Skouri-Panet, F., Li, J., Ferard, C., Gugger, M., Laurent, T., Couradeau, E., Ragon, M., Cosmidis, J., Menguy, N., Margaret-Oliver, I., Tavera, R., Lopez-Garcia, P., & Moreira, D. (2014). Intracellular Ca-carbonate biomineralization is widespread in cyanobacteria. *Proceedings of the National Academy of Sciences*, *111*, 10933–10938.

Benzerara, K., Yoon, T. H., Tyliszczak, T., Constantz, B., Spormann, A. M., & Brown, G. E. (2004). Scanning transmission X-ray microscopy study of microbial calcification. *Geobiology*, *2*, 249–259.

Beveridge, T. J. (1981). Ultrastructure, chemistry, and function of the Bacterial Wall. In G. H. Bourne, J. F. Danielli, & K. W. Jeon (Eds.), *International review of cytology* (pp. 229–317). Academic Press.

Block, K. R., O'Brien, J. M., Edwards, W. J., & Marnocha, C. L. (2021). Vertical structure of the bacterial diversity in meromictic Fayetteville Green Lake. *MicrobiologyOpen*, *10*, e1228.

Boss, S. K., & Neumann, A. (1993). Physical versus chemical processes of "whiting" formation in The Bahamas. *Carbonates and Evaporites*, *8*, 135–148.

Brandes, J. A., Wirick, S., & Jacobsen, C. (2010). Carbon *K* -edge spectra of carbonate minerals. *Journal of Synchrotron Radiation*, *17*, 676–682.

Broecker, W. (2012). Section 9. Whitings. *Geochemical Perspectives*, *1*, 249–250.

Broecker, W. S., Sanyal, A., & Takahashi, T. (2000). The origin of Bahamian Whitings revisited. *Geophysical Research Letters*, *27*, 3759–3760.

Broecker, W. S., & Takahashi, T. (1966). Calcium carbonate precipitation on the Bahama banks. *Journal of Geophysical Research (1896–1977)*, *71*, 1575–1602.

Brunner, E., Richthammer, P., Ehrlich, H., Paasch, S., Simon, P., Ueberlein, S., & van Pée, K.-H. (2009). Chitin-based organic networks: An integral part of Cell Wall biosilica in the diatom *Thalassiosira pseudonana*. *Angewandte Chemie International Edition*, *48*, 9724–9727.

Brunskill, G. J. (1969). Fayetteville Green Lake, New York. II. Precipitation and sedimentation of calcite in a meromictic lake with laminated sediments. *Limnology and Oceanography*, *14*, 830–847.

Cam, N., Georgelin, T., Jaber, M., Lambert, J.-F., & Benzerara, K. (2015). In vitro synthesis of amorphous Mg-, Ca-, Sr- and Ba-carbonates: What do we learn about intracellular calcification by cyanobacteria? *Geochimica et Cosmochimica Acta*, *161*, 36–49.

Chan, C. S., Fakra, S. C., Edwards, D. C., Emerson, D., & Banfield, J. F. (2009). Iron oxyhydroxide mineralization on microbial extracellular polysaccharides. *Geochimica et Cosmochimica Acta*, *73*, 3807–3818.

Chan, C. S., Fakra, S. C., Emerson, D., Fleming, E. J., & Edwards, K. J. (2011). Lithotrophic iron-oxidizing bacteria produce organic stalks to control mineral growth: Implications for biosignature formation. *The ISME Journal*, *5*, 717–727.

Chan, V. B. S., Johnstone, M. B., Wheeler, A. P., & Mount, A. S. (2018). Chitin facilitated mineralization in the eastern oyster. *Frontiers in Marine Science*, *5*, 347.

Chen, X., Romaniello, S. J., & Anbar, A. D. (2021). Preliminary exploration of molybdenum isotope fractionation during coprecipitation of molybdate with abiotic and microbial calcite. *Chemical Geology*, *566*, 120102.

Cosmidis, J., & Benzerara, K. (2014). Soft X-ray scanning transmission Spectromicroscopy. In E. DiMasi & L. B. Gower (Eds.), *Biomineralization sourcebook: Characterization of biominerals and biomimetic materials* (pp. 115–133). CRC Press.

Cosmidis, J., Benzerara, K., Guyot, F., Skouri-Panet, F., Duprat, E., Férard, C., Guigner, J.-M., Babonneau, F., & Coelho, C. (2015). Calcium-phosphate biomineralization induced by alkaline phosphatase activity in *Escherichia coli*: Localization, kinetics, and potential signatures in the fossil record. *Frontiers in Earth Science*, *3*, 84.

Cosmidis, J., Benzerara, K., Nassif, N., Tyliszczak, T., & Bourdelle, F. (2015). Characterization of Ca-phosphate biological materials by scanning transmission X-ray microscopy (STXM) at the Ca L2,3-, P L2,3- and C K-edges. *Acta Biomaterialia*, *12*, 260–269.

Cvetkoska, A., Hamilton, P., Ognjanova-Rumenova, N., & Levkov, Z. (2014). Observations of the genus Cyclotella (Kützing) Brébisson in ancient lakes Ohrid and Prespa and a description of two new species *C. paraocellata* sp. nov. and *C. prespanensis* sp. nov. *Nova Hedwigia*, *98*, 313–340.

DeMott, L. M., Napieralski, S. A., Junium, C. K., Teece, M., & Scholz, C. A. (2020). Microbially influenced lacustrine carbonates: A comparison of late quaternary Lahontan tufa and modern thrombolite from Fayetteville Green Lake, NY. *Geobiology*, *18*, 93–112.

Dierssen, H. M., Zimmerman, R. C., & Burdige, D. J. (2009). Optics and remote sensing of Bahamian carbonate sediment whitings and potential relationship to wind-driven Langmuir circulation. *Biogeosciences*, *6*, 487–500.

Dittrich, M., Kurz, P., & Wehrli, B. (2004). The role of autotrophic picocyanobacteria in calcite precipitation in an oligotrophic Lake. *Geomicrobiology Journal*, *21*, 45–53.

Dittrich, M., & Obst, M. (2004). Are picoplankton responsible for calcite precipitation in lakes? *AMBIO: A Journal of the Human Environment*, *33*, 559–564.

Dupraz, C., Reid, R. P., Braissant, O., Decho, A. W., Norman, R. S., & Visscher, P. T. (2009). Processes of carbonate precipitation in modern microbial mats. *Earth-Science Reviews*, *96*, 141–162.

Dupraz, C., & Visscher, P. T. (2005). Microbial lithification in marine stromatolites and hypersaline mats. *Trends in Microbiology*, *13*, 429–438.

Durkin, C. A., Mock, T., & Armbrust, E. V. (2009). Chitin in diatoms and its association with the Cell Wall. *Eukaryotic Cell*, *8*, 1038–1050.

Ehrlich, H. (2010). Chitin and collagen as universal and alternative templates in biomineralization. *International Geology Review*, *52*, 661–699.

Ehrlich, H., Motylenko, M., Sundareshwar, P. V., Ereskovsky, A., Zgłobicka, I., Noga, T., Płociński, T., Tsurkan, M. V., Wyroba, E., Suski, S., Bilski, H., Wysokowski, M., Stöcker, H., Makarova, A., Vyalikh, D., Walter, J., Molodtsov, S. L., Bazhenov, V. V., Petrenko, I., … Kurzydłowski, K. J. (2016). Multiphase biomineralization: Enigmatic invasive siliceous diatoms produce crystalline calcite. *Advanced Functional Materials*, *26*, 2503–2510.

Enyedi, N. T., Makk, J., Kótai, L., Berényi, B., Klébert, S., Sebestyén, Z., Molnár, Z., Borsodi, A. K., Leél-Őssy, S., Demény, A., & Németh, P. (2020). Cave bacteria-induced amorphous calcium carbonate formation. *Scientific Reports*, *10*, 8696.

Falini, G., & Fermani, S. (2004). Chitin mineralization. *Tissue Engineering*, *10*, 1–6.

Fuchs, A., Selmeczy, G. B., Kasprzak, P., Padisák, J., & Casper, P. (2016). Coincidence of sedimentation peaks with diatom blooms, wind, and calcite precipitation measured in high resolution by a multi-trap. *Hydrobiologia*, *763*, 329–344.

Fulton, J. M., Arthur, M. A., Thomas, B., & Freeman, K. H. (2018). Pigment carbon and nitrogen isotopic signatures in euxinic basins. *Geobiology*, *16*, 429–445.

Gibbs, R. J., Matthews, M. D., & Link, D. A. (1971). The relationship between sphere size and settling velocity. *Journal of Sedimentary Research*, *41*, 7–18.

Glunk, C., Dupraz, C., Braissant, O., Gallagher, K. L., Verrecchia, E. P., & Visscher, P. T. (2011). Microbially mediated carbonate precipitation in a hypersaline lake, big pond (Eleuthera, Bahamas). *Sedimentology*, *58*, 720–736.

Gomez, F. J., Mlewski, C., Boidi, F. J., Farías, M. E., & Gérard, E. (2018). Calcium carbonate precipitation in diatom-rich microbial mats: The Laguna Negra hypersaline lake, Catamarca, Argentina. *Journal of Sedimentary Research*, *88*, 727–742.

Görgen, S., Benzerara, K., Skouri-Panet, F., Gugger, M., Chauvat, F., & Cassier-Chauvat, C. (2021). The diversity of molecular mechanisms of carbonate biomineralization by bacteria. *Discover Materials*, *1*, 2.

Gügi, B., Le Costaouec, T., Burel, C., Lerouge, P., Helbert, W., & Bardor, M. (2015). Diatom-specific oligosaccharide and polysaccharide structures help to unravel biosynthetic capabilities in diatoms. *Marine Drugs*, *13*, 5993–6018.

Havig, J. R., Hamilton, T. L., McCormick, M., McClure, B., Sowers, T., Wegter, B., & Kump, L. R. (2017). Water column and sediment stable carbon isotope biogeochemistry of permanently redox-stratified Fayetteville Green Lake, New York, U.S.A.: Carbon isotopes at FGL. *Limnology and Oceanography*, *63*, 570–587.

Havig, J. R., McCormick, M. L., Hamilton, T. L., & Kump, L. R. (2015). The behavior of biologically important trace elements across the oxic/euxinic transition of meromictic Fayetteville Green Lake, New York, USA. *Geochimica et Cosmochimica Acta*, *165*, 389–406.

Herth, W., & Barthlott, W. (1979). The site of β-chitin fibril formation in centric diatoms. I. Pores and fibril formation. *Journal of Ultrastructure Research*, *68*, 6–15.

Hitchcock, A. (2012) aXis 2000—analysis of X-ray images and spectra. http://unicorn.mcmaster.ca/aXis2000.html

Hodell, D. A., Schelske, C. L., Fahnenstiel, G. L., & Robbins, L. L. (1998). Biologically induced calcite and its isotopic composition in Lake Ontario. *Limnology and Oceanography*, *43*, 187–199.

Hunter, S. E. (2012) *Spatio-temporal variability in the phototrophic chemocline Community at Fayetteville Green Lake (New York)* (Master Thesis). Pennsylvania State University. https://etda.libraries.psu.edu/files/final_submissions/7242

Kamennaya, N. A., Hu, P., & Jansson, C. (2020). Sedimentation of ballasted cells-free EPS in meromictic Fayetteville Green Lake. *Geobiology*, *18*, 80–92.

Kirkwood, A. E., Shea, T., Jackson, L. J., & McCauley, E. (2007). Didymosphenia geminata in two Alberta headwater rivers: An emerging invasive species that challenges conventional views on algal bloom development. *Canadian Journal of Fisheries and Aquatic Sciences*, *64*, 1703–1709.

Küchler-Krischun, J., & Kleiner, J. (1990). Heterogeneously nucleated calcite precipitation in lake constance. A short time resolution study. *Aquatic Sciences*, *52*, 176–197.

Larson, E. B., & Mylroie, J. E. (2014). A review of whiting formation in the Bahamas and new models. *Carbonates and Evaporites*, *29*, 337–347.

Lawrence, J. R., Swerhone, G. D. W., Leppard, G. G., Araki, T., Zhang, X., West, M. M., & Hitchcock, A. P. (2003). Scanning transmission

X-ray, laser scanning, and transmission electron microscopy mapping of the exopolymeric matrix of microbial biofilms. *Applied and Environmental Microbiology*, *69*, 5543–5554.

LeDuff, P., & Rorrer, G. L. (2019). Formation of extracellular β-chitin nanofibers during batch cultivation of marine diatom Cyclotella sp. at silicon limitation. *Journal of Applied Phycology*, *31*, 3479–3490.

Lehmann, J., Solomon, D., Brandes, J., Fleckenstein, H., Jacobson, C., & Thieme, J. (2009). Synchrotron-based near-edge X-ray spectroscopy of natural organic matter in soils and sediments. In N. Senesi, B. Xing, & P. M. Huang (Eds.), *Biophysico-chemical processes involving natural nonliving organic matter in environmental systems* (pp. 729–781). John Wiley & Sons, Inc..

Lisle, J. T., & Robbins, L. L. (2016). Viral lysis of photosynthesizing microbes as a mechanism for calcium carbonate nucleation in seawater. *Frontiers in Microbiology*, *7*, 1958.

Long, J., Hu, C., & Robbins, L. (2014). Whiting events in SW Florida coastal waters: A case study using MODIS medium-resolution data. *Remote Sensing Letters*, *5*, 539–547.

Long, J. S., Hu, C., Robbins, L. L., Byrne, R. H., Paul, J. H., & Wolny, J. L. (2017). Optical and biochemical properties of a Southwest Florida whiting event. *Estuarine, Coastal and Shelf Science*, *196*, 258–268.

Martignier, A., Pacton, M., Filella, M., Jaquet, J.-M., Barja, F., Pollok, K., Langenhorst, F., Lavigne, S., Guagliardo, P., Kilburn, M. R., Thomas, C., Martini, R., & Ariztegui, D. (2017). Intracellular amorphous carbonates uncover a new biomineralization process in eukaryotes. *Geobiology*, *15*, 240–253.

Metzler, R., Zhou, D., Abrecht, M., Chiou, J.-W., Guo, J., Ariosa, D., Coppersmith, S., & Gilbert, P. (2008). Polarization-dependent imaging contrast in abalone shells. *Physical Review B*, *77*, 064110.

Meyer, K. M., Macalady, J. L., Fulton, J. M., Kump, L. R., Schaperdoth, I., & Freeman, K. H. (2011). Carotenoid biomarkers as an imperfect reflection of the anoxygenic phototrophic community in meromictic Fayetteville Green Lake. *Geobiology*, *9*, 321–329.

Mitsunobu, S., Zhu, M., Takeichi, Y., Ohigashi, T., Suga, H., Makita, H., Sakata, M., Ono, K., Mase, K., & Takahashi, Y. (2014). Nanoscale identification of extracellular organic substances at the microbe–mineral interface by scanning transmission X-ray microscopy. *Chemistry Letters*, *44*, 91–93.

Monteil, C. L., Benzerara, K., Menguy, N., Bidaud, C. C., Michot-Achdjian, E., Bolzoni, R., Mathon, F. P., Coutaud, M., Alonso, B., Garau, C., Jézéquel, D., Viollier, E., Ginet, N., Floriani, M., Swaraj, S., Sachse, M., Busigny, V., Duprat, E., Guyot, F., & Lefevre, C. T. (2021). Intracellular amorphous Ca-carbonate and magnetite biomineralization by a magnetotactic bacterium affiliated to the Alphaproteobacteria. *The ISME Journal*, *15*, 1–18.

Morse, J. W., Gledhill, D. K., & Millero, F. J. (2003). CaCO3 precipitation kinetics in waters from the great Bahama bank: Implications for the relationship between bank hydrochemistry and whitings. *Geochimica et Cosmochimica Acta*, *67*, 2819–2826.

Novis, P., Schallenberg, M., Saulnier-Talbot, É., Kilroy, C., & Reid, M. (2017). The diatom Lindavia intermedia identified as the producer of nuisance pelagic mucilage in lakes. *New Zealand Journal of Botany*, *55*, 479–495.

Oduro, H., Kamyshny, A., Zerkle, A. L., Li, Y., & Farquhar, J. (2013). Quadruple sulfur isotope constraints on the origin and cycling of volatile organic sulfur compounds in a stratified sulfidic lake. *Geochimica et Cosmochimica Acta*, *120*, 251–262.

Parkhurst, D. L., & Appelo, C. A. J. (2013). Description of input and examples for PHREEQC version 3—A computer program for speciation, batch-reaction, one-dimensional transport, and inverse geochemical calculations. In *U.S. Geological Survey techniques and methods*, *book 6* (p. 497). U.S. Geological Survey.

Politi, Y., Metzler, R. A., Abrecht, M., Gilbert, B., Wilt, F. H., Sagi, I., Addadi, L., Weiner, S., & Gilbert, P. U. P. A. (2008). Transformation mechanism of amorphous calcium carbonate into calcite in the sea urchin larval spicule. *Proceedings of the National Academy of Sciences*, *105*, 17362–17366.

Purkis, S., Cavalcante, G., Rohtla, L., Oehlert, A. M., Harris, P. M., & Swart, P. K. (2017). Hydrodynamic control of whitings on great Bahama Bank. *Geology*, *45*, 939–942.

Rahman, M. A., & Halfar, J. (2014). First evidence of chitin in calcified coralline algae: New insights into the calcification process of Clathromorphum compactum. *Scientific Reports*, *4*, 6162.

Robbins, L., Yates, K., Shinn, G., & Blackwelder, P. (1996). Whitings on the great Bahama bank: A microscopic solution to a macroscopic mystery. *Bahamas Journal of Science*, *4*, 2–7.

Robbins, L. L., & Blackwelder, P. L. (1992). Biochemical and ultrastructural evidence for the origin of whitings: A biologically induced calcium carbonate precipitation mechanism. *Geology*, *20*, 464.

Robbins, L. L., Tao, Y., & Evans, C. A. (1997). Temporal and spatial distribution of whitings on great Bahama bank and a new lime mud budget. *Geology*, *25*, 947–950.

Robbins, L. L., & Yates, K. (1992). Role of microorganisms in the production of lime mud and implications for interpretation of ancient micrite deposits. *The Paleontological Society Special Publications*, *6*, 248.

Rojas, C. A., De Santiago, T. A., Park, S., Bosak, T., & Klepac-Ceraj, V. (2021). Organic electron donors and terminal electron acceptors structure anaerobic microbial communities and interactions in a permanently stratified sulfidic Lake. *Frontiers in Microbiology*, *12*, 620424.

Schultze-Lam, S., Harauz, G., & Beveridge, T. J. (1992). Participation of a cyanobacterial S layer in fine-grain mineral formation. *Journal of Bacteriology*, *174*, 7971–7981.

Schultze-Lam, S., Schultze-Lam, S., Beveridge, T. J., & Des Marais, D. J. (1997). Whiting events: Biogenic origin due to the photosynthetic activity of cyanobacterial picoplankton. *Limnology and Oceanography*, *42*, 133–141.

Shanableh, A., Al-Ruzouq, R., Gibril, M. B. A., Khalil, M. A., AL-Mansoori, S., Yilmaz, A. G., Imteaz, M. A., & Flesia, C. (2021). Potential factors that trigger the suspension of calcium carbonate sediments and whiting in a semi-enclosed gulf. *Remote Sensing*, *13*, 4795.

Shinn, E. A., Steinen, R. P., Lidz, B. H., & Swart, P. K. (1989). Whitings, a sedimentologic dilemma. *Journal of Sedimentary Research*, *59*, 147–161.

Shiraishi, F., Omori, T., Tomioka, N., Motai, S., Suga, H., & Takahashi, Y. (2020). Characteristics of $CaCO_3$ nucleated around cyanobacteria: Implications for calcification process. *Geochimica et Cosmochimica Acta*, *285*, 55–69.

Shnyukova, E. I., & Zolotareva, E. K. (2015). Diatom exopolysaccharides: A review. *International Journal on Algae*, *17*, 50–67.

Stabel, H.-H. (1986). Calcite precipitation in Lake Constance: Chemical equilibrium, sedimentation, and nucleation by algae1. *Limnology and Oceanography*, *31*, 1081–1094.

Svetličić, V., Žutić, V., Pletikapić, G., & Radić, T. M. (2013). Marine polysaccharide networks and diatoms at the nanometric scale. *International Journal of Molecular Sciences*, *14*, 20064–20078.

Swart, P. K., Oehlert, A. M., Mackenzie, G. J., Eberli, G. P., & Reijmer, J. J. G. (2014). The fertilization of the Bahamas by Saharan dust: A trigger for carbonate precipitation? *Geology*, *42*, 671–674.

Takahashi, T., Broecker, W., Li, Y. H., & Thurber, D. (1968). Chemical and isotopic balances for a meromictic Lake. *Limnology and Oceanography*, *13*, 272–292.

Thompson, J. B. (2000). Microbial Whitings. In *Microbial sediments* (pp. 250–260). Springer, Berlin, Heidelberg.

Thompson, J. B., & Ferris, F. G. (1990). Cyanobacterial precipitation of gypsum, calcite, and magnesite from natural alkaline lake water. *Geology*, *18*, 995.

Thompson, J. B., Ferris, F. G., & Smith, D. A. (1990). Geomicrobiology and sedimentology of the mixolimnion and chemocline in Fayetteville Green Lake, New York. *PALAIOS*, *5*, 52–75.

Tokura, S., Nishimura, S., & Nishi, N. (1983). Studies on chitin IX. Specific binding of calcium ions by carboxymethyl-chitin. *Polymer Journal*, *15*, 597–602.

Urbani, R., Sist, P., Pletikapić, G., Radić, T. M., Svetličić, V., & Žutic, V. (2012). Diatom polysaccharides: Extracellular production, isolation and molecular characterization. In D. N. Karunaratne (Ed.) *The complex world of polysaccharides* (pp. 345–370). IntechOpen.

Uveges, B. T., Teece, M. A., Fulton, J. M., & Junium, C. K. (2018). Environmental controls on pigment distributions in the freshwater microbialites of Fayetteville Green Lake. *Organic Geochemistry*, *125*, 165–176.

Wei, X., Chen, S., Rong, J., Sui, Z., Wang, S., Lin, Y., Xiao, J., & Huang, D. (2021). Improving the Ca(II) adsorption of chitosan via physical and chemical modifications and charactering the structures of the calcified complexes. *Polymer Testing*, *98*, 107192.

Weiner, S., Sagi, I., & Addadi, L. (2005). Choosing the crystallization path less traveled. *Science*, *309*, 1027–1028.

Winsborough, B. M. (2000). Diatoms and benthic microbial carbonates. In R. E. Riding & S. M. Awramik (Eds.), *Microbial sediments* (pp. 76–83). Springer, Berlin, Heidelberg.

Winsborough, B. M., & Golubić, S. (1987). The role of diatoms in stromatolite growth: Two examples from modern freshwater Settings1. *Journal of Phycology*, *23*, 195–201.

Wolthers, M., Nehrke, G., Gustafsson, J. P., & Van Cappellen, P. (2012). Calcite growth kinetics: Modeling the effect of solution stoichiometry. *Geochimica et Cosmochimica Acta*, *77*, 121–134.

Zerkle, A. L., Kamyshny, A., Kump, L. R., Farquhar, J., Oduro, H., & Arthur, M. A. (2010). Sulfur cycling in a stratified euxinic lake with moderately high sulfate: Constraints from quadruple S isotopes. *Geochimica et Cosmochimica Acta*, *74*, 4953–4970.

Zhu, T., & Dittrich, M. (2016). Carbonate precipitation through microbial activities in natural environment, and their potential in biotechnology: A review. *Frontiers in Bioengineering and Biotechnology*, *4*, 4.

SUPPORTING INFORMATION

Additional supporting information can be found online in the Supporting Information section at the end of this article.

How to cite this article: Stanton, C., Barnes, B. D., Kump, L. R., & Cosmidis, J. (2023). A re-examination of the mechanism of whiting events: A new role for diatoms in Fayetteville Green Lake (New York, USA). *Geobiology*, *21*, 210–228. https://doi.org/10.1111/gbi.12534